Historical (1700–2012) Global Multi-model Estimates of the Fire Emissions from the Fire Modeling Intercomparison Project (FireMIP)

Fang Li[1*], Maria Val Martin[2], Stijn Hantson[3,4], Meinrat O. Andreae[5,6], Almut Arneth[4], Gitta Lasslop[7], Chao Yue[8,9], Dominique Bachelet[10], Matthew Forrest[7], Johannes W. Kaiser[11,6], Erik Kluzek[12], Xiaohong Liu[13], Stephane Mangeon[14,15], Joe R. Melton[16], Daniel S. Ward[17], Anton Darmenov[18], Thomas Hickler[7,19], Charles Ichoku[20], Brian I. Magi[21], Stephen Sitch[22], Guido R. van der Werf[23], Christine Wiedinmyer[24]

[1] International Center for Climate and Environment Sciences, Institute of Atmospheric Physics, Chinese Academy of Sciences, Beijing, China

[2] Leverhulme Center for Climate Change Mitigation, Department of Animal & Plant Sciences, Sheffield University, Sheffield, UK

[3] Geospatial Data Solutions Center, University of California, Irvine, CA, USA

[4] Karlsruhe Institute of Technology (KIT), Institute of Meteorology and Climate research, Atmospheric Environmental Research, Garmisch-Partenkirchen, Germany

[5] Max Planck Institute for Chemistry, Mainz, Germany

[6] Senckenberg Biodiversity and Climate Research Institute (BiK-F), Senckenberganlage, Germany

[7] Department of Geology and Geophysics, King Saud University, Riyadh, Saudi Arabia

[8] State Key Laboratory of Soil Erosion and Dryland Farming on the Loess Plateau, Northwest A&F University, Yangling, Shanxi, China

[9] Laboratoire des Sciences du Climat et de l'Environnement, LSCE/IPSL, CEA-CNRS-UVSQ, Université Paris-Saclay, Gif-sur-Yvette, France

[10] Biological and Ecological Engineering, Oregon State University, Corvallis, OR, USA
[11] Deutscher Wetterdienst, Offenbach, Germany
[12] National Center for Atmospheric Research, Boulder, CO, USA
[13] Department of Atmospheric Science, University of Wyoming, Laramie, WY, USA
[14] Department of Physics, Imperial College London, London, UK
[15] Now at CSIRO, Data61, Brisbane, QLD, Australia
[16] Climate Research Division, Environment and Climate Change Canada, Victoria, BC, Canada
[17] Karen Clark and Company, Boston, MA, USA
[18] Global Modeling and Assimilation Office, NASA Goddard Space Flight Center, Greenbelt, MD, USA
[19] Department of Physical Geography, Goethe University, Frankfurt am Main, Germany
[20] Howard University, NW, Washington, DC, USA
[21] Department of Geography and Earth Sciences, University of North Carolina at Charlotte, Charlotte, NC, USA
[22] College of Life and Environmental Sciences, University of Exeter, Exeter, UK
[23] Faculty of Science, Vrije Universiteit, Amsterdam, The Netherlands
[24] University of Colorado Boulder, Boulder, CO, USA
*Correspondence to: Fang Li (lifang@mail.iap.ac.cn)

Abstract

Fire emissions are critical for carbon and nutrient cycles, climate, and air quality. Dynamic Global Vegetation Models (DGVMs) with interactive fire modeling provide important estimates for long-term and large-scale changes of fire emissions. Here we present the first multi-model estimates of global gridded historical fire emissions for 1700–2012, including carbon and 33 species of trace gases and aerosols. The dataset is based on simulations of nine DGVMs with different state-of-the-art global fire models that participated in the Fire Modeling Intercomparison Project (FireMIP), using the same and standardized protocols and forcing data, and the most up-to-date fire emission factor table from field and laboratory studies over various land cover types. We evaluate the simulations of present-day fire emissions by comparing them with satellite-based products. Evaluation results show that most DGVMs simulate present-day global fire emission totals within the range of satellite-based products. They can capture the high emissions over the tropical savannas, low emissions over the arid and sparsely vegetated regions, and the main features of seasonality. However, most models fail to simulate the interannual variability, partly due to a lack of modeling peat fires and tropical deforestation fires. Historically, all models show only a weak trend in global fire emissions before ~1850s, consistent with multi-source merged historical reconstructions as input data for CMIP5 and CMIP6. The long-term trends among DGVMs are quite different for the 20th century, with some models showing an increase and others a decrease in fire emissions, mainly as a result of the discrepancy in

their simulated responses to human population density change and land-use and land-cover change (LULCC). Our study provides an important dataset for the development of regional and global multi-source merged historical reconstructions, analyses of the historical changes of fire emissions and their uncertainties, and quantification of their role in the Earth system. It also highlights the importance of accurately modeling the responses of fire emissions to LULCC and population density change in reducing uncertainties in historical reconstructions of fire emissions and providing more reliable future projections.

1. Introduction

Fire is an intrinsic feature of terrestrial ecosystem ecology globally, and has emerged soon after the appearance of terrestrial plants over 400 million years ago (Scott and Glasspool, 2006; Bowman et al., 2009). Fire emissions play an important role in the Earth system. First, species emitted from fires are a key component of the global and regional carbon budgets (Bond-Lamberty et al., 2007; Ciais et al., 2013; Kondo et al., 2018), a major source of greenhouse gases (Tian et al., 2016), and the largest contributor of primary carbonaceous aerosols globally (Andreae and Rosenfeld, 2008; Jiang et al., 2016). Second, by changing the atmospheric composition, fire emissions affect the global and regional radiation balance and climate (Ward et al., 2012; Tosca et al. 2013; Jiang et al., 2016; Grandey et al., 2016; McKendry et al., 2018; Hamilton et al., 2018; Thornhill et al., 2018). Third, fire emissions change the terrestrial nutrient and carbon cycles through altering the deposition of nitrogen and phosphorus, surface ozone concentration, and meteorological conditions (Mahowald et al., 2008; Chen et al., 2010; McKendry et al., 2018; Yue and Unger, 2018). In addition, they degrade the air quality (Val Martin et al., 2015; Knorr et al., 2017), which poses a significant risk to human health hazard and has been estimated to result in at least ~165,000, and more likely ~339,000 pre-mature deaths per year globally (Johnston et al., 2012; Marlier et al., 2013; Lelieveld et al., 2015).

To date, only emissions from individual fires or small-scale fire complexes can be directly measured from laboratory experiments and field campaigns (Andreae and Merlet, 2001; Yokelson et al., 2013; Stockwell et al., 2016; Andreae, 2019). Regionally and globally, fire emissions are often estimated based on satellite observations, fire proxies, and/or numerical models, even though some attempts have been made to bridge the gap between local observations and regional estimations using combinations of aircraft and ground based measurements from observation campaigns (e.g. SAMBBA, ARCTAS), satellite-based inventories, and chemical transport models (Fisher et al., 2010; Reddington et al., 2019; Konovalov et al., 2018). Satellite-based fire emission estimates are primarily derived from satellite observations of burned area, active fire counts, fire radiative power, and/or constrained by satellite observations of aerosol optical depth (AOD), CO, or CO_2 (Wiedinmyer et al., 2011; Kaiser et al., 2012; Krol et al., 2013; Konovalov et al., 2014; Ichoku and Ellison, 2014; Darmenov and da Silva, 2015; van der Werf et al., 2017; Heymann et al., 2017). Satellite-based fire emission estimates are available globally, but only cover the present-day period, i.e. since 1997 for GFED and shorter periods for others. Fire emission histories have been inferred from a variety of proxies, such as ice-core records of CH_4 (isotope $\delta^{13}CH_4$ from pyrogenic or biomass burning source), black carbon, levoglucosan, vallic acid, ammonium, and CO (Ferretti et al., 2005; McCornnell et al., 2007; Conedera et al., 2009; Wang et al., 2012; Zennaro et al., 2014), site-level sedimentary charcoal records (Marlon et al., 2008, 2016), visibility records (van Marle et al., 2017a), and fire-scar records (Falk et al. 2011). The fire proxies can be used to reconstruct historical fire emissions on a local to global scale and for time periods of decades to millennia and beyond. However, fire proxies are of limited spatial extent and cannot be directly converted into emission amount. Moreover, large uncertainties and discrepancies were shown in their referred regional or global long-term trends due to limited sample size and often unclear representative area and time period of fire emissions (Pechony and Shindell, 2010; van der Werf et al., 2013; Legrand et al., 2016).

Dynamic Global Vegetation Models (DGVMs) that include fire modeling are indispensable for estimating fire carbon emissions at global and regional scales and for past, present, and future periods (Hantson et al., 2016). These models represent interactions among fire dynamics, biogeochemistry, biogeophysics, and vegetation dynamics at the land surface in a physically and chemically consistent modeling framework. DGVMs also constitute the terrestrial ecosystem component of Earth System models (ESMs) and have been widely used in global change research (Levis et al., 2004; Li et al., 2013; Kloster and Lasslop, 2017). Fire emissions of trace gases and aerosols can be derived from fire carbon emissions simulated by DGVMs and fire emission factors which depend on species and land cover type (Li et al., 2012; Knorr et al., 2016).

Modeling fire and fire emissions within DGVMs started in the early 2000s (Thonicke et al., 2001), and has rapidly progressed during the past decade (Hantson et al., 2016). The Fire Model Intercomparison Project (FireMIP) initiated in 2014 was the first international collaborative effort to better understand the behavior of global fire models (Hantson et al., 2016), where a set of common fire modeling experiments driven by the same forcing data were performed (Rabin et al., 2017). Nine DGVMs with different state-of-the-art global fire models participated in FireMIP. All global fire models used in the upcoming 6th Coupled Model Intercomparison Project (CMIP6) and IPCC AR6 were included in FireMIP, except for the fire scheme in GFDL-ESM (Rabin et al., 2018; Ward et al., 2018) which is similar to that of CLM4.5 (Li et al., 2012) in FireMIP. Furthermore, GlobFIRM (Thonicke et al., 2001) in FireMIP was the most commonly-used fire scheme in CMIP5 (Kloster and Lasslop, 2017).

Earlier studies provided a single time series of fire emissions for global grids or regions (Schultz et al., 2008; Mieville et al., 2010; Lamarque et al., 2010; Marlon et al., 2016; van Marle et al., 2017b; and references therein). This limits their utility for quantifying the uncertainty in global and regional reconstructions of fire emissions and its subsequent impacts on estimated historical changes in carbon cycle, climate, and air pollution. A small number of studies also investigated the drivers of fire carbon emission trends (Kloster et al., 2010; Yang et al., 2014; Li et al., 2018; Ward et al., 2018). However, because only a single DGVM was used in these studies, they could not identify the uncertainty source in recent model-based reconstructions or help understand the inter-model discrepancy in projections of future fire emissions.

The present study provides a new dataset of global gridded fire emissions, including carbon and 33 species of trace gases and aerosols, over the 1700–2012 time period, based on nine DGVMs with different state-of-the-art global fire models that participated in FireMIP. This dataset provides a basis for developing multi-source (satellite-based products, model simulations, and/or fire proxies) merged fire emission reconstructions and methods. It also, for the first time, allows end users to select all or a subset of model-based reconstructions that best suits their regional or global research needs. Importantly, it enables the quantification of the uncertainty range of past fire emissions and their impacts. In addition, the model-based estimates of fire emissions are comprehensively evaluated through comparison with satellite-based products, including amounts, spatial distribution, seasonality, and interannual variability, providing information on the limitations of recent model-based reconstructions. We also analyze long-term trends of the model-based reconstructions, and the forcing drivers of these trends for each DGVM and for inter-model differences.

2 Methods and datasets

2.1 Models in FireMIP

Nine DGVMs with different fire modules participated in FireMIP: CLM4.5 with CLM5 fire module, CTEM, JSBACH-SPITFIRE, JULES-INFERNO, LPJ-GUESS-GlobFIRM, LPJ-GUESS-SIMFIRE-BLAZE, LPJ-GUESS-SPITFIRE, MC2, and ORCHIDEE-SPITFIRE (Table 1, see Rabin et al., 2017 for detailed description of each model). JSBACH, ORCHIDEE, and LPJ-GUESS used the variants of SPITFIRE (Thonicke et al., 2010) with updated representation of human ignitions and suppression, fuel moisture, combustion completeness, and the relationship between spread rate and wind speed for JSBACH (Lasslop et al., 2014), combustion completeness for ORCHIDEE (Yue et al., 2014, 2015), and human ignition, post-fire mortality factors, and modifications for matching tree age/size structure for LPJ-GUESS (Lehsten et al., 2009; Rabin et al., 2017).

The global fire models in the nine DGVMs have diverse levels of complexity (Rabin et al., 2017). SIMFIRE is a statistical model based on present-day satellite-based fire products (Knorr et al., 2016). In CLM4.5, crop, peat, and tropical deforestation fires are empirically/statistically modeled (Li et al., 2013). The scheme for fires outside the tropical closed forests and croplands in CLM4.5 (Li et al., 2012; Li and Lawrence, 2017) and fire modules in CTEM (Arora and Boer, 2005; Melton and Arora, 2016), GlobFIRM (Thonicke, 2001), and INFERNO (Mangeon et al., 2016) are process-based and of intermediate-complexity. That is, area burned is determined by two processes: fire occurrence and fire spread, but with simple empirical/statistical equations for each process. Fire modules in MC2 (Bachelet et al., 2015; Sheehan et al., 2015) and SPITFIRE variants are more complex, which use the Rothermel equations (Rothermel, 1972) to model fire spread and consider the impact of fuel composition on fire behavior.

How humans affect fires differs among these global fire models (Table 2), which influences their estimates of fire emissions. GlobFIRM does not consider any direct human effect on fires and MC2 fire model only considers human suppression on fire. CLM4.5 includes modeling of crop fires, human deforestation and degradation fires in tropical closed forests, and human ignitions and suppression on both occurrence and spread of fires for regions outside of tropical closed forests and croplands. Burned area in SIMFIRE and human influence on fire occurrence in other models are a non-linear function of population density. CTEM and JSBACH-SPITFIRE also consider human suppression on fire duration. JULES-INFERNO treats cropland and crop fires as natural grassland and grassland fires. MC2 doesn't include crop PFTs, and models crop fires as fires in natural vegetation regions. All models, except for CLM4.5 and INFERNO, set burned area to zero over cropland. FireMIP models treat pasture fires as natural grassland fires by using the same parameter values if they have pasture plant functional types (PFTs) or lumping pastures with natural grasslands otherwise. Note that biomass harvest is considered in pastures in LPJ-GUESS-GlobFIRM and LPJ-GUESS-SIMFIRE-BLAZE, which decreases fuel availability for fires, and that JSBACH-SPITFIRE sets high fuel bulk density for pasture PFTs.

Only CLM4.5 simulates peat fires, although only emissions from burning of vegetation tissues and litter are included in outputs for FireMIP (i.e. burning of soil organic matter is not included) (Table 2).

In the FireMIP models, fire carbon emissions are calculated as the product of burned area, fuel load, and combustion completeness. Combustion completeness is the fraction of live plant tissues and ground litter burned (0–100%). It depends on PFT and plant tissue type in GlobFIRM and in the fire modules of CLM4.5 and CTEM, and also a function of soil moisture in INFERNO. Combustion completeness depends on plant tissue type and surface fire intensity in SIMFIRE, fuel type and wetness in the SPITFIRE family models, and fuel type, load, and moisture in MC2 fire module.

2.2 FireMIP experimental protocol and input datasets

The nine DGVMs in FireMIP are driven with the same forcing data (Rabin et al., 2017). The atmospheric forcing is from CRU-NCEP v5.3.2 with a spatial resolution of 0.5° and a 6-hourly temporal resolution (Wei et al., 2014). The 1750–2012 annual global atmospheric CO_2 concentration is derived from ice core and NOAA monitoring station data (Le Quéré et al., 2014). Annual LULCC and population density at a 0.5° resolution for 1700–2012 are from Hurtt et al. (2011) and Klein Goldewijk et al. (2010, HYDE v3.1), respectively. Monthly cloud-to-ground lightning frequency for 1901–2012, at 0.5° resolution, is derived from the observed relationship between present-day lightning and convective available potential energy (CAPE) anomalies (Pfeiffer et al., 2013, J. Kaplan, personal communication, 2015).

Fire emissions in this study are estimated using the model outputs of PFT-level fire carbon emissions and vegetation characteristics (PFTs and their fractional area coverages) from the FireMIP historical transient control run (SF1) (Rabin et al., 2017). SF1 includes three phases (Fig. 1): the 1700 spin-up phase, the 1701–1900 transient phase, and the 1901–2012 transient phase. In the 1700 spin-up phase, all models are spun up to equilibrium, forced by population density and prescribed land-use and land-cover change (LULCC) at their 1700 values, 1750 atmospheric CO_2 concentration, and the repeatedly cycled 1901–1920 atmospheric forcing (precipitation, temperature, specific humidity, surface pressure, wind speed, and solar radiation) and lightning data. The 1701–1900 transient phase is forced by 1701–1900 time-varying population and LULCC, with constant CO_2 concentration at 1750 level until 1750 and time-varying CO_2 concentration for 1750–1900, and the cycled 1901–1920 atmospheric forcing and lightning data. In the 1901–2012 transient phase, models are driven by 1901–2012 time-varying population density, LULCC, CO_2 concentration, atmospheric forcing, and lightning data. Unlike all other models, MC2 and CTEM run from 1901 and 1861, respectively, rather than 1700.

Six FireMIP models (CLM4.5, JSBACH-SPITFIRE, JULES-INFERNO, LPJ-GUESS-SPITFIRE, LPJ-GUESS-SIMFIRE-BLAZE, and ORCHIDEE-SPITFIRE) also provide outputs of five sensitivity simulations: constant climate, constant atmospheric CO_2 concentration, constant land cover, constant population density, and constant lightning frequency throughout the whole simulation period. The sensitivity simulations are helpful for understanding the drivers of changes in reconstructed fire emissions.

2.3 Estimates of fire trace gas and aerosol emissions

Based on fire carbon emissions and vegetation characteristics from DGVMs and fire emission factors, fire emissions of trace gas and aerosol species i and the PFT j, $E_{i,j}$ (g species m^{-2} s^{-1}), are estimated according to Andreae and Merlet (2001):

$$E_{i,j} = \mathrm{EF}_{\mathrm{i,j}} \times CE_j/[\mathrm{C}], \quad (1)$$

where $\mathrm{EF}_{\mathrm{i,j}}$ (g species (kg dry matter (DM)) $^{-1}$) is a PFT-specific emission factor (EF), CE_j denotes the fire carbon emissions of PFT j (g C m^{-2} s^{-1}), and [C]=0.5×10^3 g C (kg DM)$^{-1}$ is a unit conversion factor from carbon to dry matter.

The EFs used in this study (Table 3) are based on Andreae and Merlet (2001), with updates from field and laboratory studies over various land cover types published during 2001–2018 (Andreae, 2019). All FireMIP model simulations used the same EFs from Table 3..

DGVMs generally simulate vegetation as mixture of PFTs in a given grid location to represent plant function at global scale, instead of land cover types. In Table 4, we associate the PFTs from each DGVM to the land cover types shown in Table 3. Grass, shrub, savannas, woodland, pasture, tundra PFTs are classified as grassland/savannas. Tree PFTs and crop PFTs are classified as forests and cropland, respectively, similar to Li et al. (2012), Mangeon et al. (2016), and Melton and Arora (2016). PFTs of other broadleaf deciduous tree in CTEM, extra-tropical evergreen and deciduous tree in JSBACH, and broadleaf deciduous tree and needleleaf evergreen tree in JULES are divided into tropical, temperate, and boreal groups following Nemani and Running (1996).

We provide two versions of fire emission products with different spatial resolutions: the original spatial resolution for each FireMIP DGVM outputs (Table 1), and a 1x1 degree horizontal resolution. For the latter, fire emissions are unified to 1 degree resolution using bilinear interpolation for CLM4.5, CTEM, JSBACH, and JULES which have coarser resolution, and area-weighted averaging-up for other models whose original resolution is 0.5 degree. The 1x1 degree product is used for present-day evaluation and historical trend analyses in Sects. 3 and 4.

2.4 Benchmarks

Satellite-based products are commonly used as benchmarks to evaluate present-day fire emission simulations (Rabin et al., 2017, and references therein). In the present study, six satellite-based products are used (Table 5). Fire emissions in GFED4/GFED4s (small fires included in GFED4s) (van der Werf et al., 2017), GFAS1 (Kaiser et al., 2012), and FINN1.5 (Wiedinmyer et al., 2011) are based on emission factor (EF) and fire carbon emissions (CE) (Eq. 1). CE is estimated from MODIS burned area and VIRS/ATSR active fire products in the GFED family, MODIS active fire detection in FINN1.5, and MODIS fire radiative power (FRP) in GFAS1. Fire emissions from FEER1 (Ichoku and Ellison, 2014) and QFEDv2.5 (Darmenov and da Silva, 2015) are derived using FRP, and constrained with satellite AOD observations. Satellite-based present-day fire emissions for the same region can differ by a factor of 2–4 on an annual basis (van der Werf et al., 2010) and up to 12 on a monthly basis (Zhang et al., 2014). The discrepancy among satellite-based estimates of present-day fire emissions mainly comes from the satellite observations used, the methods applied for deriving fire emissions, and emissions factors.

2.5 Multi-source merged historical reconstructions

We also compared the simulated historical changes with historical reconstructions merged from multiple sources used as forcing data for CMIPs. Fire emission estimates for CMIP5 and CMIP6 were merged from different sources (Table 5). For CMIP5 (Lamarque et al., 2010), the decadal fire emissions are available from 1850 to 2000, estimated using GFED2 fire emissions (van der Werf et al., 2006) for 1997 onwards, RETRO (Schultz et al., 2008) for 1960–1900, GICC (Mieville et al., 2010) for 1900-1950, and kept constant at the 1900 level for 1850–1900. RETRO combined literature reviews with satellite-based fire products and the GlobFIRM fire model. GICC is based on a burned area reconstruction from literature review and sparse tree ring records (Mouillot et al., 2005), satellite-based fire counts, land cover map, and representative biomass density and burning efficiency of each land cover type.

For CMIP6, monthly fire emission estimates are available from 1750 to 2015 (van Marle et al., 2017b). The CMIP6 estimates are merged from GFED4s fire carbon emissions for 1997 onwards, charcoal records GCDv3 (Marlon et al., 2016) for North America and Europe, visibility records for Equatorial Asia (Field et al., 2009) and central Amazon (van Marle et al., 2017b), and the median of simulations of six FireMIP models (CLM4.5, JSBACH-SPITFIRE, JULES-INFERNO, LPJ-GUESS-SPITFIRE, LPJ-GUESS-SIMFIRE-BLAZE, and

ORCHIDEE-SPITFIRE) for all other regions. Then, based on the merged fire carbon emissions, CMIP6 fire trace gas and aerosols emissions are derived using EF from Andreae and Merlet (2001) with updates to 2013 and Akagi et al. (2011) with updates for temperate forests to 2014, and a present-day land cover map.

3 Evaluation of present-day fire emissions

The spatial pattern and temporal variability of different fire emission species are similar, with slight differences resulting from the estimated fire carbon emissions from the land cover types that have different emission factors (Table 3). Therefore, we focus on several important species as examples to exhibit the performance of FireMIP models on the simulations of present-day fire emissions.

3.1 Global amounts and spatial distributions

As shown in Table 6, FireMIP models, except for MC2 and LPJ-GUESS-GlobFIRM, estimate present-day fire carbon, CO_2, CO, CH_4, BC, OC, and $PM_{2.5}$ annual emissions to be within the range of satellite-based products. For example, the estimated range of fire carbon emissions is 1.7–3.0 Pg C yr^{-1}, whereas it is 1.5–4.2 Pg C yr^{-1} for satellite-based products. Low fire emissions in MC2 result from relatively low simulated global burned area, only about 1/4 of satellite-based observations (Andela et al., 2017). In contrast, high emissions in LPJ-GUESS-GlobFIRM are mainly due to the higher combustion completeness of woody tissues (70–90% of stem and coarse woody debris burned in post-fire regions) than those used in other FireMIP models (Table 2) and the satellite-based GFED family (20–40% for stem and 40–60% for coarse woody debris) (van der Werf et al., 2017).

FireMIP DGVMs, except for MC2, represent the general spatial distribution of fire emissions evident in satellite-based products, with high fire BC emissions over tropical savannas and low emissions over the arid and sparsely vegetated regions (Fig. 2). Among the nine models, CLM4.5, JULES-INFERNO, and LPJ-GUESS-SIMFIRE-BLAZE have higher global spatial pattern correlation with satellite-based products than the other models, indicating higher skill in their spatial-pattern simulations. It should also be noted that, on a regional scale, CTEM, JULES-INFERNO, LPJ-GUESS-SPITFIRE, and ORCHIDEE-SPITFIRE underestimate fire emissions over boreal forests in Asia and North America. LPJ-GUESS-GlobFIRM and LPJ-GUESS-SIMFIRE-BLAZE overestimate fire emissions over the Amazon and African rainforests. CLM4.5 and JSBACH-SPITFIRE overestimate fire emissions over eastern China and North America, respectively. MC2 underestimates fire emissions over most regions, partly because it allows only one ignition per year per grid cell and thus underestimates the burned area.

We further analyze the spatial distribution of inter-model difference. As shown in Fig. 3, the main disagreement among FireMIP models occurs in the tropics, especially over the tropical savannas in Africa, South America, and northern Australia. This is mainly driven by MC2, CTEM, JSBACH-SPITFIRE, and ORCHIDEE-SPITFIRE simulations (Fig. 2). Difference among the satellite-based estimates has a similar spatial pattern, but higher than inter-model spread in savannas over southern Africa and lower in the temperate arid and semi-arid regions and at the North of 60ºN over Eurasia (Fig. S1a).

3.2 Seasonal cycle

The FireMIP models reproduce similar seasonality features of fire emissions to satellite-based products, that is, peak month is varied from the dry season in the tropics to the warm season in the extra-tropics (Fig. 4).

For the tropics in the Southern Hemisphere, fire PM2.5 emissions of satellite-based products peak in August–September. Most FireMIP models can reproduce this pattern, except ORCHIDEE-SPITFIRE and LPJ-GUESS-SPITFIRE peaking two months and one month earlier, respectively, and JSBACH-SPITFIRE with much lower amplitude of seasonal variability likely caused by parameter setting in its fuel moisture functions (Table S9 in Rabin et al. 2016).

For the tropics in the Northern Hemisphere, most FireMIP models exhibit larger fire emissions in the northern winter, consistent with the satellite-based products.

In the northern extra-tropical regions, satellite-based products show two periods of high values: April–May resulting mainly from fires over croplands and grasslands, and July mainly due to fires over the boreal evergreen forests. Most FireMIP models can reproduce the second one, except for LPJ-GUESS-SPITFIRE which peaks in October. CLM4.5 is the only model that can captures both peak periods partly because it’s the only one to model the crop fires.

3.3 Interannual variability

Global fire $PM_{2.5}$ emissions from satellite-based products for 1997–2012 show a substantial interannual variability, which peaks in 1997–1998, followed by a low around 2000 and a decline starting in 2002/2003 (Fig. 5). The 1997–1998 high emission values are caused by peat fires in Equatorial Asia in 1997 and widespread drought-induced fires in 1998 associated with the most powerful El Niño event in 1997–1998 recorded in history (van der Werf et al., 2017; Kondo et al., 2018). Most FireMIP models cannot reproduce the 1997–1998 peak, except for CLM4.5 as the only model that simulates the burning of plant-tissue and litter from peat fires (although burning of soil organic matter is not included) and the drought-linked tropical deforestation and degradation fires (Li et al., 2013, Kondo et al., 2018). CLM4.5, CTEM, and LPJ-GUESS-SIMFIRE-BLAZE present the highest temporal correlation between models and satellite-based products (0.55–0.79 for CLM4.5, 0.51–0.68 for CTEM, and 0.39–0.72 for LPJ-GUESS-SIMFIRE-BLAZE), and thus are more skillful than other models to reproduce the interannual variability observed from satellite-based products (Table 7).

We use the coefficient of variation (CV, the standard deviation divided by the mean, %) to represent the amplitude of interannual variability of fire emissions. As shown in Fig. 5, for 1997–2012, all FireMIP models underestimate the variation as a result of (at least) partially missing the 1997–1998 fire emission peak. For 2003–2012 (the common period of all satellite-based products and models), interannual variation of annual fire $PM_{2.5}$ emissions in CLM4.5, CTEM, and LPJ-GUESS family models lies within the range of satellite-based products (CV=6–12%). Other models present weaker variation (CV=5%) except for MC2 (CV=24%) that has a much stronger variation than all satellite-based products and other FireMIP models.

4 Historical changes and drivers

4.1 Historical changes

Figure 6 shows historical simulations of the FireMIP models and the CMIP reconstructions for fire carbon, CO_2, CO, and $PM_{2.5}$ emissions. We find similar historical changes for all the species, with the maximum global fire emissions given by LPJ-GUESS-GlobFIRM and the minima by LPJ-GUESS-SPITFIRE before 1901 and MC2 afterwards.

Long-term trends in modeled global fire emissions for all models are weak before the1850s (relative trend <0.015% yr^{-1}). They are similar to CMIP6 estimates (Fig. 6), but in disagreement with earlier reconstructions based on charcoal records (Marlon et al., 2008; Marlon et al., 2016), ice-core CO records (Wang et al., 2010), and ice-core $\delta^{13}CH_4$ records (Ferretti et al., 2005), which exhibit a rapid increase from 1700 to roughly the 1850s.

After the1850s, disagreement in the trends among FireMIP models begins to emerge. Fire emissions in LPJ-GUESS-SIMFIRE-BLAZE decline since ~1850, while fire emissions in LPJ-GUESS-SPITFIRE, MC2, and ORCHIDEE-SPITFIRE show upward trends from ~1900s. In CLM4.5, CTEM, and JULES-INFERNO, fire emissions increase slightly before ~1950, similar to the CMIP6 estimates, but CTEM and JULES-INFERNO decrease thereafter, contrary to CMIP5 and CMIP6 estimates and CLM4.5. JSBACH-SPITFIRE simulates a decrease of fire emissions before 1940s and an increase later, similar to the CMIP5 estimates. All the long-term trends described above are significant at the 0.05 level using the Mann-Kendall trend test.

Earlier reconstructions based on fire proxies also show a big difference in long-term changes after the 1850s. The reconstruction based on the Global Charcoal Database version 3 (GCDv3, Marlon et al., 2016) exhibits a decline from the late 19th century to the 1920s, and then an upward trend until ~1970, followed by a drop. The reconstructions based on the GCDv1 (Marlon et al., 2008) and ice-core CO records (Wang et al., 2010) show a sharp drop since roughly the 1850s, while a steady rise is exhibited in the reconstruction based on ice-core $\delta^{13}CH_4$ records (Ferretti et al., 2005). The simulated historical changes of the FireMIP models (Fig. 6) fall into this fairly broad range of long-term trends in these reconstructions.

Spatial patterns of inter-model spread of fire emissions for 1700–1850 and 1900–2000 (Figs. S1b-c) are similar to the present-day pattern as shown in Fig. 3.

4.2 Drivers

Six FireMIP models also conducted sensitivity experiments, which can be used to identify the drivers of their long-term trends during the 20th century. The six models are also used for building CMIP6 fire emission estimates (van Marle et al. 2017b). As shown in Figs. 6 and 7, the downward trend of global fire emissions in LPJ-GUESS-SIMFIRE-BLAZE is mainly caused by LULCC and increasing population density. Upward trends in LPJ-GUESS-SPITFIRE and ORCHIDEE-SPITFIRE are dominated by LULCC and rising population density and CO_2 during the 20th century. In CLM4.5 and JULES-INFERNO, upward trends before ~1950 are attributed to rising CO_2, climate change, and LULCC, and the subsequent drop in JULES-INFERNO mainly results from the rising population density and climate change. Long-term changes of global fire emissions in JSBACH-SPITFIRE are mainly driven by LULCC and rising CO_2.

As shown in Fig. 7, the inter-model spread in long-term trends mainly arises from the simulated anthropogenic influence (LULCC and population density change) on fire emissions, as the standard deviation in simulated responses to LULCC (0.27 Pg C yr^{-1}) and population density (0.11 Pg C yr^{-1}) is much larger than the other drivers.

LULCC decreases global fire emissions sharply in LPJ-GUESS-SIMFIRE-BLAZE during the 20th century, but increases global fire emissions for the other models except for JSBACH-SPITFIRE. The response to LULCC in LPJ-GUESS-SIMFIRE-BLAZE is because it assumes no fire in croplands and accounts for biomass harvest which decreases fuel availability in pastures (Table 2), the area of which expanded over the 20th century. The LULCC-induced increase in fire emissions for ORCHIDEE-SPITFIRE, LPJ-GUESS-SPITFIRE, and JULES-INFERNO are partly caused by increased burned area due to the expansion of grassland (pastures are lumped in grassland in these models) where fuels are easier to burn than woody vegetation in the model setups (Rabin et al., 2017). CLM4.5 models crop fires and tropical deforestation and degradation fires. Crop fire emissions in

CLM4.5 are estimated to increase during the 20th century due to expansion of croplands and increased fuel loads over time (Fig. S2). Emissions of tropical deforestation and degradation fires in CLM4.5 are increased before ~1950, responding to increased human deforestation rate in tropical closed forests based on prescribed land use and land cover changes (Li et al. 2018). In JSBACH-SPITFIRE, as croplands and pastures expand over time, the assumption of no fires over croplands tends to decrease fire emissions, while the setting of high fuel bulk density for pastures tends to increase fire emissions due to increased fuel combusted per burned area, which together partly result in the shifted sign of response to LULCC around the 1940s.

Rising population density throughout the 20th century decreases fire emissions in CLM4.5 and LPJ-GUESS-SIMFIRE-BLAZE because they include human suppression on both fire occurrence and fire spread. Fire suppression increases with rising population density simulated explicitly in CLM4.5 and implicitly in LPJ-GUESS-SIMFIRE-BLAZE. On the contrary, rising population density increases fire emissions in LPJ-GUESS-SPITFIRE and ORCHIDEE-SPITFIRE because observed human suppression on fire spread found in Li et al. (2013), Hantson et al. (2015), and Andela et al. (2017) is not taken into account in the two models. The response to population density change for the other models is small, reflecting the compensating effects of human ignition and human suppression on fire occurrence (strongest in JULES-INFERNO in FireMIP models), and human suppression on fire duration (JSBACH-SPITFIRE).

All models simulate increased fire emissions with increased CO_2 since elevated CO_2 increases fuel load through increasing the carbon entering into the land ecosystems (Mao et al., 2009) and improving the water-use efficiency (Keenan et al., 2013). Such a CO_2-driven increase of fuel load is consistent with a recent analysis of satellite-derived vegetation indices (Zhu et al., 2016). FireMIP models also agree that impacts of changes in lightning frequency on long-term trends of fire emissions are small. Moreover, most FireMIP models agree that climate change tends to increase fire carbon emissions during the first several decades and then falls, reflecting co-impacts of climate on both fuel load and fuel moisture.

4.3 Regional long-term changes

We divided the global map into 14 regions following the definition of the GFED family (Fig. 8a). As shown in Fig. 8b, inter-model discrepancy in long-term changes are largest in Southern Hemisphere South America (SHSA), southern and northern Africa (NHAF and SHAF), and central Asia (CEAS).

Most FireMIP models reproduce the upward trends of fire CO emissions found also in the CMIP5 or CMIP6 estimates since 1950s in SHSA and till ~1950 in Africa (Figs. 9e, h, and i). Long-term trends in regional fire emissions in SHSA, Africa, and central Asia can broadly explain the upward trends in global fire emissions in LPJ-GUESS-SPITFIRE, MC2, and ORCHIDEE-SPITFIRE, the downward trends in LPJ-GUESS-SIMFIRE-BLAZE, and the rise followed by a drop in CTEM, whose global fire emissions exhibit most obvious long-term trends in FireMIP models (Fig. 6).

In other regions, the difference in long-term changes among models is smaller (Fig. 9). Emissions of most models and CMIP5 estimates exhibit a significant decline in temperate North America (TENA) from ~1850 to ~1970, while historical changes of CMIP6 estimates are comparatively small (Fig. 9b). LPJ-GUESS-SIMFIRE-BLAZE has a more obvious long-term change than the other FireMIP models and CMIPs in boreal North America (BONA) and northern South America (NHSA) (Figs. 9a and d). MC2 and LPJ-GUESS-GlobFIRM emissions increase since the 1900s in Europe (EURO), while remain overall constant for other models and CMIPs (Fig. 9f). In boreal Asia (BOAS), emissions of most models and CMIP6 are relatively constant, while LPJ-GUESS-GlobFIRM and CMIP5 emissions decline form 1850 to the 1950s and from 1900 to the 1970s, respectively, and then rise (Fig. 9j). JULES, LPJ-GUESS-SIMFIRE-BLAZE, CLM4.5, CTEM, and CMIP6 emissions significantly decline since the 1950s in Southeast Asia (SEAS), while CMIP5 emissions increase (Fig. 9l). In equatorial Asia (EQAS), CMIPs emissions increase after ~1950 , but in FireMIP only CLM4.5 partly reproduces it (Fig. 9m). As shown in Figs. S3-5, long-term changes of regional fire emissions for other species are similar to those of fire CO emissions.

The long-term changes and inter-model disagreement of regional fire emissions are mainly caused by simulated responses to LULCC and/or population density change for the 20th century (Fig. S6-19). Besides, climate change also plays an important role in North America, northern South America, Europe, northern Africa, boreal and central Asia, and Australia for some FireMIP models. FireMIP models generally simulate increased regional fire emissions with increased CO_2 concentration and negligible impacts due to changes in lightning frequency, similar to the responses of global fire emissions.

5 Summary and outlook

Our study provides new multi-model reconstructions of global historical fire emissions for 1700–2012, including carbon and 33 species of trace gases and aerosols. Two versions of the fire emission product are available, at the original spatial resolution for outputs of each FireMIP model and at a unified 1x1 degree. The dataset is based on simulations of fire carbon emissions and vegetation distribution from nine DGVMs with state-of-the-art global fire models that participated in FireMIP and the most up-to-date emission factors over various land cover types. It will be available to the public at https://bwfilestorage.lsdf.kit.edu/public/projects/imk-ifu/FireMIP/emissions.

Our study provides an important dataset with wide-ranging applications for Earth science research communities. First, it is the first multi-model-based reconstruction of fire emissions, and can serve as the basis for further developing multi-source merged products of global and regional fire emissions and the merging methodology. van Marle et al. (2017b) presented an example for using part of the dataset to develop a multi-source merged fire emission product as forcing dataset for CMIP6. In van Marle et al. (2017b), the median of fire carbon emissions from six FireMIP models was used to determine historical changes over most regions of the world. The merging method and merged product in van Marle et al. (2017b) are still preliminary, and need to be improved in the future, e.g. by weighting the different models depending on their global or regional simulation skills. Secondly, our dataset includes global gridded reconstructions for 300 years, thus can be used for analyzing global and regional historical changes in fire emissions on inter-annual to multi-decadal time scales and their interplay with climate variability and human activities. Third, the fire emission reconstructions based on multiple models provide, for the first time, a chance to quantify and understand the uncertainties in historical changes of fire emissions and their subsequent impacts on carbon cycle, radiative balance, air quality, and climate. Hamilton et al. (2018), for example, used fire emission simulations from two global fire models and the CMIP6 estimates to drive an aerosol model. This allowed for quantification of the impact of uncertainties in pre-industrial fire emissions on estimated pre-industrial aerosol concentrations and historical radiative forcing.

This study also provides significant information of the recent state of fire model performance by evaluating the present-day estimates based on FireMIP fire models (also those used in the upcoming CMIP6). Our results show that most FireMIP models can overall reproduce the amount, spatial pattern, and seasonality of fire emissions shown by satellite-based fire products. Yet they fail to simulate the interannual variability partly due to a lack of modeling peat and tropical deforestation fires. In addition, Teckentrup et al. (2019) found that climate was the main driver of interannual variability for the FireMIP models. A good representation of fire duration may be important to get the response of fire emissions to climate right. However, all FireMIP models limit their fire duration of individual fire events within one day over natural vegetation regions, so they cannot skillfully model the drought-induced large fires that last multiple days (Le Page et al., 2015; Ward et al., 2018). Recently, Andela et al. (2018) derived a dataset of fire duration from MODIS satellite observations, which provides a valuable dataset for developing parameterization of fire duration in global fire models.

This study also identifies population density and LULCC as the primary uncertainty sources in fire emission estimates. Therefore, accurately modeling these responses remains a top priority to reduce uncertainty in historical reconstructions and future projections of fire emissions, especially given that modeling is the only way for future projections. For the response to changes in population density, many FireMIP models have not included the observed relationship between population density and fire spread (Table 2). Moreover, Bistinas et al. (2014) and Parisien et al. (2016) reported obvious spatial heterogeneity of the population density–burned area relationship that is poorly represented in FireMIP models.

For the response to LULCC, improving the modeling of crop fires, pasture fires, deforestation and degradation fires, and human indirect effect on fires (e.g. fragmentation of the landscape) and reducing the difference in interpretation of land use data set in models are critical. Fire has been widely used in agricultural management during the harvesting, post-harvesting, or pre-planting periods (Korontzi et al., 2006; Magi et al., 2012), whose emissions are an important source of greenhouse gas and air pollutant emissions (Tian et al., 2016; Wu et al., 2017; Andreae, 2019). GFED4s reported that fires in croplands contributed 5% of burned area and 6% of fire carbon emissions globally in the present day (Randerson et al., 2012; van der Werf et al., 2017). In FireMIP, only CLM4.5 simulates crop fires, whereas the other models assume no fire in croplands or treat croplands as natural grassland. In CLM4.5, crop fires contribute 5% of 2000-2010 global burned area, the same as the GFED4s estimates, but emit 260 Tg C yr^{-1} carbon emissions (contribution rate:13%), higher than GFED4s (138 Tg C yr^{-1}) because CLM4.5 simulates higher fuel loads in croplands than the CASA model used by GFED4s. Carbon emissions from crop fires and the contribution of crop fire emissions to the total fire emissions in CLM4.5 increase over the 20th century (Fig. S2), consistent with earlier estimates based on different crop fire scheme (Ward et al., 2018). For FireMIP models which exclude croplands from burning, expansion of croplands leads to a decrease in burned area and fire carbon emissions. JULES-INFERNO treats croplands as natural grasslands. Grasses dry out faster than woody vegetation and are easier to burn in model setups, so increasing cropland area leads to increasing burned area and fire carbon emissions. Different treatment of crop fires can contribute to the uncertainty in simulated fire emissions. Because four out of six FireMIP models used for generating CMIP6 estimates exclude croplands from burning (van Marle et al., 2017b), CMIP6 estimates may underestimate the impact of historical changes of crop fire emissions in some regions (e.g. China, Russia, India). Given the small extent of crop fires, high resolution remote sensing may help improve the detection of crop fires (Randerson et al., 2012; Zhang et al., 2018), which can benefit the driver analyses and modeling of historical crop fires and their emissions in DGVMs.

Le Page et al. (2017) and Li et al. (2018) highlighted the importance of tropical deforestation and degradation fires in the long-term changes of reconstructed and projected global fire emissions, but only CLM4.5 in FireMIP models estimate the tropical deforestation and degradation fires. For pasture fires, all FireMIP models assume that they are as natural grassland fires, which needs to be verified by, for example, satellite-based products. If fires over pastures and natural grasslands are significantly different, adding the gridded coverage of pasture as a new input field in DGVMs without pasture PFTs and developing a parameterization of pasture fires will be necessary. Furthermore, Archibald (2016) and Andela et al. (2017) found that expansion of croplands and pastures decreased fuel continuity and thus reduced burned area and fire emissions. However, no FireMIP model parameterizes this indirect human effect on fires. In addition, DGVMs generalize the global vegetation using different PFTs (Table 4) and represent land use data in different way, which may lead to different response of fire emissions to LULCC and thus different long-term changes of fire emissions among model simulations, given that many parameters and functions in global fire models are PFT-dependent (Rabin et al. 2016). LUH2 used in LUMIP and ongoing CMIP6 provide information of forest/non-forest coverage changes (Lawrence et al., 2016), which can reduce the misinterpretation of the land use data in models and thus the inter-model spread of fire emission changes.

Since most FireMIP models do not consider the human suppression on fire spread and the decrease in fuel continuity from expanding croplands and pastures, these models, and hence CMIP6 estimates that are mainly based on them, may underestimate fire emissions and their downward trend over the Industrial Era. This underestimation may thus affect the estimation of the radiative forcing of fire emissions and the historical response of trace gas and aerosol concentrations, temperature, precipitation, and energy, water, and biogeochemical cycles to fire emissions in Earth/Climate system models which include these fire models or are driven by such fire emissions. It may also influence future projections of climate and Earth system responses to various population density and land use scenarios.

Author contribution. FL contributed to the processing and analyses of the fire emission dataset. SS and AA designed the FireMIP experiments and LF, SH, GL, CY, DB, SM, MF, JM, and TH performed FireMIP simulations. MA compiled the EF table. JK, AD, CI, Gv, CW provided satellite-based and CMIP estimates of fire emissions. FL prepared the first draft of manuscript, and revised it with contributions from all co-authors.

Acknowledgements. This study is co-supported by the National Key R&D Program of China (2017YFA0604302 and 2017YFA0604804), National Natural Science Foundation of China (41475099 and 41875137), and CAS Key Research Program of Frontier Sciences (QYZDY-SSW-DQC002). MVM is supported by the US Joint Fire

Science Program (13-1-01-4) and the UK Leverhulme Trust through a Leverhulme Research Centre Award (RC-2015-029). AA acknowledges support from the Helmholtz Association, its ATMO programme and the Impulse and Networking fund which funded initial FireMIP activities. AA and SH acknowledge also the EU FP7 project BACCHUS (603445). GL is funded by the German Research Foundation (338130981). BIM is supported by NSF (BCS-1436496). CI is supported by NASA (NNH12ZDA001N-IDS). We are grateful to Stéphane Mangeon for providing data of JULES-INFERNO simulations, and R. J. Yokelson, Z.-D. Lin, S. Kloster, M. van Marle, B. Bond-Lamberty, and J. R. Marlon for helpful discussions.

Competing interests. The authors declare that they have no conflict of interest.

References

Akagi, S. K., Yokelson, R. J., Wiedinmyer, C., Alvarado, M. J., Reid, J. S., Karl, T., Crounse, J. D., and Wennberg, P. O.: Emission factors for open and domestic biomass burning for use in atmospheric models, Atmos. Chem. Phys., 11, 4039-4072, https://doi.org/10.5194/acp-11-4039-2011, 2011.

Andela, N., et al. : A human-driven decline in global burned area, Science, 356, 1356-1362, 2017.

Andela, N., Morton, D. C., Giglio, L., Paugam, R., Chen, Y., Hanson, S., van der Werf, G. R., and Randerson, J. T.: The Global Fire Atlas of individual fire size, duration, speed, and direction, Earth Syst. Sci. Data Dis., https://doi.org/10.5194/essd-2018-89, in review, 2018.

Andreae, M. O.: Emission of trace gases and aerosols from biomass burning – an updated assessment, Atmos. Chem. Phys., 19, 8523-8546, https://doi.org/10.5194/acp-19-8523-2019, 2019.

Andreae, M. O. and Merlet, P.: Emission of trace gases and aerosols from biomass burning, Global Biogeochem. Cy., 15, 955–966, 2001.

Andreae, M. O. and Rosenfeld, D.: Aerosol–cloud– precipitation interactions, Part 1, The nature and sources of cloud-active aerosols, Earth-Sci. Rev., 89, 13–41, doi:10.1016/j.earscirev.2008.03.001, 2008.

Archibald, S.: Managing the human component of fire regimes: lessons from Africa, Philos. T. R. Soc. B., 371, 20150346, 2016.

Arora, V. K. and Boer, G.: Fire as an interactive component of dynamic vegetation models, J. Geophys. Res., 110, 2005.

Bachelet, K. Ferschweiler, T. J. Sheehan, B. M. Sleeter, and Z. Zhu: Projected carbon stocks in the conterminous USA with land use and variable fire regimes, Glob. Change Biol., 21, 4548–4560, 2015.

Best, M. J., et al.: The Joint UK Land Environment Simulator (JULES), model description – Part 1: Energy and water fluxes, Geosci. Model Dev., 4, 677–699, doi:10.5194/gmd-4-677-2011, http://www.geosci-model-dev.net/4/677/2011/, 2011.

Bistinas, S. P. Harrison, I. C. Prentice, and J. M. C. Pereira: Causal relationships versus emergent patterns in the global controls of fire frequency, Biogeosciences, 11, 5087–5101, 2014.

Bond-Lamberty, B., Peckham, S.D., Ahl, D.E., and Gower, S.T.:The dominance of fire in determining carbon balance of the central Canadian boreal forest, Nature, 450, 89–92, 2007.

Bowman, D. M. J. S., et al.: Fire in the Earth system, Science, 324, 481–484, 2009.

Brovkin, V.,et al.: Effect of anthropogenic land-use and land-cover changes on climate and land carbon storage in CMIP5 projections for the twenty-first century, J. Climate, 26, 6859–6881, doi:10.1175/JCLI-D-12-00623.1, http://journals.ametsoc.org/doi/abs/10.1175/JCLI-D-12-00623.1, 2013.

Chen, Y., Randerson, J., van der Werf, G., Morton, D., Mu, M., and Kasibhatla, P.: Nitrogen deposition in tropical forests from savanna and deforestation fires, Glob. Change Biol., 16, 2024–2038, 2010.

Ciais, P., C., et al.: Carbon and Other Biogeochemical Cycles, In: Climate Change 2013: The Physical Science Basis. Contribution of Working Group I to the Fifth Assessment Report of the Intergovernmental Panel on Climate Change, edited by: Stocker, T.F., Qin,D., Plattner, G.-K., Tignor, M., Allen, S.K., Boschung, J., Nauels, A., Xia, Y., Bex, V., and Midgley, P. M., Cambridge University Press, Cambridge, United Kingdom and New York, NY, USA, 467–544, 2013.

Clark, D. B. et al.: The Joint UK Land Environment Simulator (JULES), model description Part 2: Carbon fluxes and vegetation dynamics, Geosci. Model Dev., 4, 701–722, doi:10.5194/gmd-4-701-2011, http://www.geosci-model-dev.net/4/701/2011/, 2011.

Conedera, M., Tinner,W., Neff, C., Meurer, M., Dickens, A. F., and Krebs, P.:

Reconstructing past fire regimes: methods, applications, and relevance to fire management and conservation, Quat. Sci. Rev., 28, 555–576, doi:10.1016/j.quascirev.2008.11.005, 2009.

Darmenov, A. S., and da Silva, A.: The Quick Fire Emissions Dataset (QFED): Documentation of versions 2.1, 2.2 and 2.4, In: Technical Report Series on Global Modeling and Data Assimilation, edited by Koster, R. D., NASA Goddard Space Flight Center; Greenbelt, MD, USA, pp. 212, 2015.

Falk, D. A., Heyerdahl, E. K., Brown, P. M., Farris, C., Fulé, P. Z., McKenzie, D., Swetnam, T. W., Taylor, A. H., and Van Horne, M. L.: Multi-scale controls of historical forest-fire regimes: new insights from fire-scar networks, Front. Ecol. Environ., 9, 446–454, 2011.

Ferretti, D. F., et al. : Unexpected changes to the global methane budget over the past 2000 years, Science, 309, 1714–1717, https://doi.org/10.1126/science.1115193, 2005.

Field, R. D., van der Werf, G. R., and Shen, S. S. P.: Human amplification of drought-induced biomass burning in Indonesia since 1960, Nat. Geosci., 2, 185–188, https://doi.org/10.1038/ngeo443, 2009.

Fisher, J. A., et al.: Source attribution and interannual variability of Arctic pollution in spring constrained by aircraft (ARCTAS, ARCPAC) and satellite (AIRS) observations of carbon monoxide, Atmos. Chem. Phys., 10, 977-996, https://doi.org/10.5194/acp-10-977-2010, 2010.

Grandey, B. S., Lee, H.-H., and Wang, C.: Radiative effects of interannually varying vs. interannually invariant aerosol emissions from fires, Atmos. Chem. Phys., 16, 14495-14513, https://doi.org/10.5194/acp-16-14495-2016, 2016.

Hamilton, D. S., et al.: Reassessment of pre-industrial fire emissions strongly affects anthropogenic aerosol forcing, Nat. Commun., 9, 3182, doi: 10.1038/s41467-018-05592-9, 2018.

Hantson, S., Pueyo, S., and Chuvieco, E.: Global fire size distribution is driven by human impact and climate, Global Ecol. Biogeogr., 24, 77–86, 2015.

Hantson, S., et al.: The status and challenge of global fire modelling, Biogeosciences, 13, 3359–3375, doi:10.5194/bg-13-3359-2016, 2016.

Heymann, J., Reuter, M., Buchwitz, M., Schneising, O., Bovensmann, H., Burrows, J. P., Massart, S., Kaiser, J. W., and Crisp, D.: CO_2 emission of Indonesian fires in 2015 estimated from satellite-derived atmospheric CO_2 concentrations, Geophys. Res. Lett., 44, 1537–1544, 2017.

Hurtt, G. C., et al.: Harmonization of land-use scenarios for the period 1500–2100: 600 years of global gridded annual land-use transitions, wood harvest, and resulting secondary lands, Climatic Change, 109, 117–161, doi:10.1007/s10584-011-0153-2, 2011.

Ichoku, C. and Ellison, L.: Global top-down smoke-aerosol emissions estimation using satellite fire radiative power measurements, Atmos. Chem. Phys., 14, 6643-6667, https://doi.org/10.5194/acp-14-6643-2014, 2014.

Jiang, Y., Lu, Z., Liu, X. Qian, Y., Zhang, K., Wang, Y., and Yang, X.: Impacts of global wildfire aerosols on direct radiative, cloud and surface-albedo forcings simulated with CAM5, Atmos. Chem. Phys., 16, 14805-14824, 2016

Johnston, F. H., et al.: Estimated global mortality attributable to smoke from landscape fires, Environ. Health Persp., 120, 695–701. https://doi.org/10.1289/ehp.1104422, 2012.

Kaiser, J. W., Heil, A., Andreae, M. O., Benedetti, A., Chubarova, N., Jones, L., Morcrette, J.-J., Razinger, M., Schultz, M. G., Suttie, M., and van der Werf, G. R.: Biomass burning emissions estimated with a global fire assimilation system based on observed fire radiative power, Biogeosciences, 9, 527–554, https://doi.org/10.5194/bg-9-527-2012, 2012.

Keenan, T. F., Hollinger, D. Y., Bohrer, G., Dragoni, D., Munger, J. W., Schmid, H. P., and Richardson, A. D.: Increase in forest water-use efficiency as atmospheric carbon dioxide concentrations rise, Nature, 499, 324–327, 2013.

Klein Goldewijk, K., Beusen, A., and Janssen, P.: Long-term dynamic modeling of global population and built-up area in a spatially explicit way: HYDE 3.1, Holocene, 20, 565–573, https://doi.org/10.1177/0959683609356587, 2010.

Kloster, S., and Lasslop, G.: Historical and future fire occurrence (1850 to 2100) simulated in CMIP5 Earth System Models, Global Planet. Change, 58-69, 2017.

Kloster, S., Mahowald, N. M., Randerson, J. T., Thornton, P. E., Hoffman, F. M., Levis, S., Lawrence, D. M.: Fire dynamics during the 20^{th} century simulated by the Community Land Model. Biogeosciences, 7(6), 1877–1902. https://doi.org/10.5194/bg-7-1877-2010, 2010.

Knorr, W., Dentener, F., Lamarque, J.-F., Jiang, L., and Arneth, A.: Wildfire air pollution hazard during the 21st century, Atmos. Chem. Phys., 17, 9223-9236, https://doi.org/10.5194/acp-17-9223-2017, 2017.

Knorr,W., Jiang, L., and Arneth, A.: Climate, CO_2 and human population impacts on global wildfire emissions, Biogeosciences, 13, 267–282, https://doi.org/10.5194/bg-13-267-2016, 2016.

Kondo, M., et al.: Land use change and El Niño-Southern Oscillation drive decadal carbon balance shifts in Southeast Asia, Nat. Commun., 9, 1154, doi: 10.1038/s41467-018-03374-x, 2018.

Konovalov, I. B., Lvova, D. A., Beekmann, M., Jethva, H., Mikhailov, E. F., Paris, J.-D., Belan, B. D., Kozlov, V. S., Ciais, P., and Andreae, M. O.: Estimation of black carbon emissions from Siberian fires using satellite observations of absorption and extinction optical depths, Atmos. Chem. Phys., 18, 14889-14924, https://doi.org/10.5194/acp-18-14889-2018, 2018.

Konovalov, I. B., Berezin, E. V., Ciais, P., Broquet, G., Beekmann, M., Hadji- Lazaro, J., Clerbaux, C., Andreae, M. O., Kaiser, J. W., and Schulze, E.: Constraining CO_2 emissions from open biomass burning by satellite observations of co-emitted species: a method and its application to wildfires in Siberia, Atmos. Chem. Phys., 14, 10383–10410, 2014.

Krinner, G., Viovy, N., de Noblet-Ducoudré, N., Ogée, J., Polcher, J., Friedlingstein, P., Ciais, P., Sitch, S., and Prentice, I. C.: A dynamic global vegetation model for studies of the coupled atmosphere-biosphere system, Global Biogeochem. Cy., 19, 1–33, https://doi.org/10.1029/2003GB002199, 2005.

Krol, M., Peters, W., Hooghiemstra, P., George, M., Clerbaux, C., Hurtmans, D., McInerney, D., Sedano, F., Bergamaschi, P., El Hajj, M., Kaiser, J. W., Fisher, D., Yershov, V., and Muller, J.-P.: How much CO was emitted by the 2010 fires around Moscow? Atmos. Chem. Phys., 13(9):4737–4747, 2013.

Lamarque, J.-F., et al.: Historical (1850–2000) gridded anthropogenic and biomass burning emissions of reactive gases and aerosols: methodology and application, Atmos. Chem. Phys., 10, 7017-7039, https://doi.org/10.5194/acp-10-7017-2010, 2010.

Lasslop, G., Thonicke, K., and Kloster, S.: SPITFIRE within the MPI Earth system model: Model development and evaluation, J. Adv. Model Earth Sy., 6, 740–755, https://doi.org/10.1002/2013MS000284, 2014.

Lawrence, D. M., et al.: The Land Use Model Intercomparison Project (LUMIP) contribution to CMIP6: rationale and experimental design, Geosci. Model Dev., 9, 2973-2998, https://doi.org/10.5194/gmd-9-2973-2016, 2016.

Legrand, M., et al.: Boreal fire records in Northern Hemisphere ice cores: a review, Clim. Past, 12, 2033-2059, https://doi.org/10.5194/cp-12-2033-2016, 2016.

Lehsten, V., Tansey, K., Balzter, H., Thonicke, K., Spessa, A., Weber, U., Smith, B., and Arneth, A.: Estimating carbon emissions from African wildfires, Biogeosciences, 6, 349-360, https://doi.org/10.5194/bg-6-349-2009, 2009.

Lelieveld, J., Evans, J. S., Fnais, M., Giannadaki, D., and Pozzer, A.: The contribution of outdoor air pollution sources to premature mortality on a global scale, Nature, 525, 367– 371, 2015.

Le Page, Y., Morton, D., Bond-Lamberty, B., Pereira, J. M. C., and Hurtt, G.: HESFIRE: A global fire model to explore the role of anthropogenic and weather drivers, Biogeosciences, 12, 887–903, https://doi.org/10.5194/bg-12-887-2015, 2015.

Le Quéré, C.,et al.: Global carbon budget 2013, Earth Syst. Sci. Data, 6, 235–263, doi:10.5194/essd-6-235-2014, http://www.earth-syst-sci-data.net/6/235/2014/, 2014.

Levis, S., Bonan, G. B., Vertenstein, M., and Oleson, K. W.: The Community Land Model's dynamic global vegetation model (CLM-DGVM): Technical description and user's guide, NCAR Tech. Note TN-459 IA, Terrestrial Sciences Section, Boulder, Colorado, 2004

Li, F., Zeng, X.-D., Levis, S.: A process-based fire parameterization of intermediate complexity in a Dynamic Global Vegetation Model, Biogeosciences, 9, 2761–2780, 2012.

Li, F., Levis, S., and Ward, D.S.: Quantifying the role of fire in the Earth system–Part 1: Improved global fire modeling in the Community Earth System Model (CESM1), Biogeosciences, 10, 2293–2314, 2013.

Li, F., and Lawrence, D.M.: Role of fire in the global land water budget during the 20th century through changing ecosystems, J. Clim., 30, 1893–908, 2017.

Li, F., Lawrence, D.M., Bond-Lamberty, B.: Human impacts on 20th century fire dynamics and implications for global carbon and water trajectories, Glob. Planet. Change, 162, 18-27, 2018.

Lindeskog, M., Arneth, A., Bondeau, A.,Waha, K., Seaquist, J., Olin, S., and Smith, B.: Implications of accounting for land use in simulations of ecosystem carbon cycling in Africa, Earth Syst. Dynam,, 4, 385–407, doi:10.5194/esd-4-385-2013, 2013.

Magi, B.I., Rabin, S., Shevliakova, E., Pacala, S.: Separating agricultural and non-agricultural fire seasonality at regional scales, Biogeosciences, 9, 3003–3012, 2012.

Mahowald, N., et al.: Global distribution of atmospheric phosphorus sources, concentrations and deposition rates, and anthropogenic impacts, Global Biogeochem. Cy., 22, GB4026, doi: 10.1029/2008GB003240, 2008.

Mangeon, S., Voulgarakis, A., Gilham, R., Harper, A., Sitch, S., and Folberth, G.: INFERNO: a fire and emissions scheme for the UK Met Office's Unified Model, Geosci. Model Dev., 9, 2685–2700, doi:10.5194/gmd-9-2685-2016, http://www.geosci-model-dev.net/9/2685/2016/, 2016.

Mao, J. F., Wang, B., and Dai, Y. J.: Sensitivity of the carbon storage of potential vegetation to historical climate variability and CO_2 in continental China, Adv. Atmos. Sci., 26, 87–100, 2009.

Marlier, M. E., DeFries, R. S., Voulgarakis, A., Kinney, P. L., Randerson, J. T., Shindell, D. T., Chen, Y., and Faluvegi, G.: El Niño and health risks from landscape fire emissions in southeast Asia, Nat. Clim. Change, 3, 131–136, 2013.

Marlon, J. R., et al.: Climate and human influences on global biomass burning over the past two millennia, Nat. Geosci., 1, 697–702, https://doi.org/10.1038/ngeo313, 2008.

Marlon, J. R., et al.: Reconstructions of biomass burning from sediment–charcoal records to improve data–model comparisons, Biogeosciences, 13, 3225–3244, https://doi.org/10.5194/bg-13-3225-2016, 2016.

McKendry, I. G., Christen, A., Lee, S.-C., Ferrara, M., Strawbridge, K. B., O'Neill, N., and Black, A.: Impacts of an Intense Wildfire Smoke Episode on Surface Radiation, Energy and Carbon Fluxes in Southwestern British Columbia, Canada, Atmos. Chem. Phys. Dis., https://doi.org/10.5194/acp-2018-252, in review, 2018.

McMeeking, G. R., et al.: Emissions of trace gases and aerosols during the open combustion of biomass in the laboratory, J. Geophys. Res.,114, D19210, doi:10.1029/2009JD011836, 2009.

Melton, J. R., and Arora, V. K.: Competition between plant functional types in the Canadian Terrestrial Ecosystem Model (CTEM) v. 2.0, Geosci. Model Dev., 9, 323–361, doi:10.5194/gmd-9-323-2016, 2016.

Mieville, A., Granier, C., Liousse, C., Guillaume, B., Mouillot, F., Lamarque, J.-F., Grégoire, J.-M., and Pétron, G.: Emissions of gases and particles from biomass burning during the 20th century using satellite data and an historical reconstruction, Atmos. Environ., 44, 1469–1477, https://doi.org/10.1016/j.atmosenv.2010.01.011, 2010.

Mouillot, F. and Field, C. B.: Fire history and the global carbon budget: a 1º×1ºfire history reconstruction for the 20th century, Glob. Change Biol., 11, 398–420, https://doi.org/10.1111/j.1365-2486.2005.00920.x, 2005.

Nemani, R.R., and Running, S.W.: Implementation of a hierarchical global vegetation classification in ecosystem function models, J. Veg. Sci., 7, 337-346, 1996.

Oleson, K., et al..: Technical Description of version 4.5 of the Community Land Model (CLM), Tech. Rep. NCAR/TN-503+STR NCAR, Boulder, CO, USA, pp.434, 2013.

Parisien, M., Miller, C., Parks, S.A., DeLancey, E.R., Robinne, F., and Flannigan, M. D.: The spatially varying influence of humans on fire probability in North America, Environ. Res. Lett., 11:075005, 2016.

Pechony, O., and Shindell, D.T.: Driving forces of global wildfires over the past millennium and the forthcoming century, P. Natl. Acad. Sci. USA, 107, 19167–19170, 2010.

Pfeiffer, M., Spessa, A., and Kaplan, J. O.: A model for global biomass burning in preindustrial time: LPJ-LMfire (v1.0), Geosci. Model Dev., 6, 643–685, doi:10.5194/gmd-6-643-2013, 2013.

Rabin, S. S., et al.: The Fire Modeling Intercomparison Project (FireMIP), phase 1: experimental and analytical protocols with detailed model descriptions. Geosci. Model Dev., 10, 1175-1197, 2017.

Rabin, S. S., Ward, D. S., Malyshev, S. L., Magi, B. I., Shevliakova, E., and Pacala, S. W.: A fire model with distinct crop, pasture, and non-agricultural burning: use of new data and a model-fitting algorithm for FINAL.1, Geosci. Model Dev., 11, 815-842, https://doi.org/10.5194/gmd-11-815-2018, 2018.

Reddington, C. L., Morgan, W. T., Darbyshire, E., Brito, J., Coe, H., Artaxo, P., Scott, C. E., Marsham, J., and Spracklen, D. V.: Biomass burning aerosol over the Amazon: analysis of aircraft, surface and satellite observations using a global aerosol model, Atmos. Chem. Phys., 19, 9125-9152, https://doi.org/10.5194/acp-19-9125-2019, 2019.

Rothermel, R. C.:A mathematical model for predicting fire spread in wildland fuels, Res. Pap. INT-115, US Department of Agriculture, Ogden, UT, USA, pp. 40, 1972.

Schultz, M. G., Heil, A., Hoelzemann, J. J., Spessa, A., Thonicke, K., Goldammer, J. G., Held, A. C., Pereira, J. M. C., and van het Bolscher, M.: Global wildland fire emissions from 1960 to 2000, Global Biogeochem. Cy., 22, GB2002, https://doi.org/10.1029/2007GB003031, 2008.

Scott, A. C., and Glasspool, I. J.: The diversification of Palaeozoic fire systems and fluctuations in atmospheric oxygen concentration, Proc. Natl. Acad. Sci. U.S.A., 103, 10861–10865, doi:10.1073/pnas.0604090103, 2006.

Sheehan, T., Bachelet, D., and Ferschweiler, K.: Projected major fire and vegetation changes in the Pacific Northwest of the conterminous United States under selected CMIP5 climate futures, Ecol. Model., 317, 16–29, doi:10.1016/j.ecolmodel.2015.08.023, 2015.

Smith, B., Wårlind, D., Arneth, A., Hickler, T., Leadley, P., Siltberg, J., and Zaehle, S.: Implications of incorporating N cycling and N limitations on primary production in an individual-based dynamic vegetation model, Biogeosciences, 11, 2027–2054, doi:10.5194/bg-11-2027-2014, 2014.

Stockwell, C. E., et al.: Nepal Ambient Monitoring and Source Testing Experiment (NAMaSTE): emissions of trace gases and light-absorbing carbon from wood and dung cooking fires, garbage and crop residue burning, brick kilns, and other sources, Atmos. Chem. Phys., 16, 11043-11081, 2016.

Thonicke, K., Spessa, A., Prentice, I. C., Harrison, S. P., Dong, L., and Carmona-Moreno, C.: The influence of vegetation, fire spread and fire behaviour on biomass burning and trace gas emissions: Results from a process-based model, Biogeosciences, 7, 1991–2011, 2010.

Thonicke, K., Venevsky, S., Sitch, S., and Cramer, W.: The role of fire disturbance for global vegetation dynamics: Coupling fire into a Dynamic Global Vegetation Model, Global Ecol. Biogeogr., 10, 661–677, 2001.

Thornhill, G. D., Ryder, C. L., Highwood, E. J., Shaffrey, L. C., and Johnson, B. T.: The effect of South American biomass burning aerosol emissions on the regional climate, Atmos. Chem. Phys., 18, 5321-5342, https://doi.org/10.5194/acp-18-5321-2018, 2018.

Tian, H., et al.: The terrestrial biosphere as a net source of greenhouse gases to the atmosphere, Nature, 531, 225–228, 2016.

Tosca, M. G., Randerson, J. T., and Zender, C. S.: Global impact of smoke aerosols from landscape fires on climate and the Hadley circulation, Atmos. Chem. Phys., 13, 5227–5241, https://doi.org/10.5194/acp-13-5227-2013, 2013.

Teckentrup, L., Harrison, S. P., Hantson, S., Heil, A., Melton, J. R., Forrest, M., Li, F., Yue, C., Arneth, A., Hickler, T., Sitch, S., and Lasslop, G.: Sensitivity of simulated historical burned area to environmental andanthropogenic controls: A comparison of seven fire models, Biogeosciences Discuss., https://doi.org/10.5194/bg-2019-42, 2019.

Val Martin, M., Heald, C.L., Lamarque, J.F., Tilmes, S., Emmons, L.K., Schichtel, B.A.: How emissions, climate, and land use change will impact mid-century air quality over the United States: a focus on effects at national parks, Atmos. Chem. Phys. 15, 2805-2823, 2015.

van der Werf, G. R., Peters, W., van Leeuwen, T. T., and Giglio, L: What could have caused pre-industrial biomass burning emissions to exceed current rates?, Clim. Past, 9, 289–306, http://www.clim-past.net/9/289/2013/, 2013.

van der Werf, G. R., Randerson, J. T., Giglio, L., Collatz, G. J., Mu, M., Kasibhatla, P. S., Morton, D. C., DeFries, R. S., Jin, Y., and van Leeuwen, T. T.: Global fire emissions and the contribution of deforestation, savanna, forest, agricultural, and peat fires (1997–2009), Atmos. Chem. Phys., 10, 11707–11735, https://doi.org/10.5194/acp-10-11707-2010, 2010.

van der Werf, G. R., et al.: Global fire emissions estimates during 1997–2016, Earth Syst. Sci. Data., 9, 679-720, 2017.

van Marle, M. J. E., Field, R. D., van der Werf, G. R., Estrada de Wagt, I. A., Houghton, R. A., Rizzo, L. V., Artaxo, P., and Tsigaridis, K.: Fire and deforestation dynamics in Amazonia (1973–2014), Global Biogeochem. Cy., 31, 24–38,https://doi.org/10.1002/2016GB005445, 2017a.

van Marle, M. J. E., et al., Historic global biomass burning emissions based on merging satellite observations with proxies and fire models (1750 - 2015), Geosci. Model Dev. , 10, 3329-3357, doi:10.5194/gmd-2017-32, 2017b.

Wang, Z., et al.: The isotopic record of Northern Hemisphere atmospheric carbon monoxide since 1950: implications for the CO budget, Atmos. Chem. Phys., 12, 4365–4377, https://doi.org/10.5194/acp-12-4365-2012, 2012.

Ward, D. S., Kloster, S., Mahowald, N. M., Rogers, B.M., Randerson, J. T., Hess, P. G.: The changing radiative forcing of fires: Global model estimates for past, present and future, Atmos. Chem. Phys. 12, 10857–10886, 2012.

Ward, D. S., Shevliakova, E., Malyshev, S., Rabin, S.: Trends and variability of global fire emissions due to historical anthropogenic activities. Global Biogeochem. Cy.,32, 122–142, https://doi.org/10.1002/2017GB005787, 2018.

Wei, Y., et al.: The North American Carbon Program Multi-scale Synthesis and Terrestrial Model Intercomparison Project – Part 2: Environmental driver data, Geoscientific Model Development, 7, 2875–2893, doi:10.5194/gmd-7-2875-2014, 2014.

Wiedinmyer, C., Akagi, S. K., Yokelson, R. J., Emmons, L. K., Al- Saadi, J. A., Orlando, J. J., and Soja, A. J. : The Fire INventory from NCAR (FINN): A high resolution global model to estimate the emissions from open burning, Geosci. Model Dev., 4, 625–641, https://doi.org/10.5194/gmd- 4- 625- 2011, 2011

Wu, Y., Han, Y., Voulgarakis, A., Wang, T., Li, M., Wang, Y., Xie, M., Zhuang, B., and Li, S.: An agricultural biomass burning episode in eastern China: Transport, optical properties, and impacts on regional air quality, J. Geophys. Res.-Atmos., 122, 2304–2324, doi:10.1002/2016JD025319, 2017.

Yang, J., Tian, H., Tao, B., Ren, W., Kush, J., Liu, Y., and Wang, Y.: Spatial and temporal patterns of global burned area in response to anthropogenic and environmental factors: Reconstructing global fire history for the 20th and early 21st centuries, J. Geophys. Res, -Biogeo., 119, 249–263. https://doi.org/10.1002/2013JG002532, 2014.

Yokelson, R. J., et al.: Coupling field and laboratory measurements to estimate the emission factors of identified and unidentified trace gases for prescribed fires, Atmos. Chem. Phys., 13, 89–116, doi:10.5194/acp-13-89-2013, 2013.

Yue, C., Ciais, P., Cadule, P., Thonicke, K., and van Leeuwen, T. T.: Modelling the role of fires in the terrestrial carbon balance by incorporating SPITFIRE into the global vegetation model ORCHIDEE– Part 2: Carbon emissions and the role of fires in the global carbon balance, Geosci. Model Dev., 8, 1321–1338, https://doi.org/10.5194/gmd-8-1321-2015, 2015.

Yue, C., et al.: Modelling the role of fires in the terrestrial carbon balance by incorporating SPITFIRE into the global vegetation model ORCHIDEE – Part 1: simulating historical global burned area and fire regimes, Geosci. Model Dev., 7, 2747–2767, https://doi.org/10.5194/gmd-7-2747-2014, 2014.

Yue, X., and Unger, N. : Fire air pollution reduces global terrestrial productivity, nature commun., 9, 5413, https://doi.org/10.1038/s41467-018-07921-4, 2018.

Zennaro, P., et al.: Fire in ice: two millennia of boreal forest fire history from the Greenland NEEM ice core, Clim. Past, 10, 1905–1924, https://doi.org/10.5194/cp-10-1905-2014, 2014.

Zhang, F., Wang, J., Ichoku, C., Hyer, E. J., Yang, Z., Ge, C., Su, S., Zhang, X., Kondragunta, S., Kaiser, J. W., Wiedinmyer, C., and da Silva, A.: Sensitivity of mesoscale modeling of smoke direct radiative effect to the emission inventory: a case study in northern sub-Saharan African region, Environ. Res. Lett., 9, 075002, doi:10.1088/1748-9326/9/7/075002, 2014.

Zhang, T. R., Wooster, M. J., de Jong, M. C., and Xu, W. D.: How well does the 'Small Fire Boost' methodology used within the GFED4.1s fire emissions database represent the timing, location and magnitude of agricultural burning? Remote. Sens., 10, 823, doi:10.3390/rs10060823, 2018.

Zhu, Z., et al: Greening of the Earth and its drivers, Nat. Clim. Change, 6, 791–795, 2016.

Table 1. Summary description of the Dynamic Global Vegetation Models (DGVMs) participated in FireMIP.

DGVMs	tem. res. of model outputs	spatial res. of model outputs	period	natural veg. distrib.	fire scheme ref.	DGVM ref.
CLM4.5 but CLM5 fire model (CLM4.5)	monthly	~1.9° (lat) ×2.5° (lon)	1700–2012	P	Li et al. (2012, 2013) Li and Lawrence (2017)	Oleson et al. (2013)
CTEM	monthly	2.8125°	1861–2012	P	Arora and Boer (2005) Melton and Arora 2016	Melton and Arora (2016)
JSBACH-SPITFIRE (JSBACH)	monthly	1.875°	1700–2012	P	Lasslop et al. (2014) Thonicke et al. (2010)	Brovkin et al. (2013)
JULES-INFERNO (JULES)	monthly	~1.2° (lat) ×1.9°(lon)	1700–2012	M	Mangeon et al. (2016)	Best et al. (2011) Clark et al. (2011)
LPJ-GUESS-GlobFIRM (LGG)	annual	0.5°	1700–2012	M	Thonicke et al. (2001)	Smith et al. (2014) Lindeskog et al. (2013)
LPJ-GUESS-SPITFIRE (LGS)	monthly	0.5°	1700–2012	M	Lehsten et al. (2009) Rabin et al. (2017)	Smith et al. (2001) Ahlstrom et al. (2012)
LPJ-GUESS-SIMFIRE -BLAZE (LGSB)	monthly	0.5°	1700–2012	M	Knorr et al. (2016)	Smith et al. (2014) Lindeskog et al. (2013) Nieradzik et al. (2017)
MC2	annual	0.5°	1901–2008	M	Bachelet et al. (2015) Sheehan et al. (2015)	Bachelet et al. (2015) Sheehan et al. (2015)
ORCHIDEE-SPITFIRE (ORCHIDEE)	monthly	0.5°	1700–2012	P	Yue et al. (2014, 2015) Thonicke et al. (2010)	Krinner et al. (2005)

Acronym: CLM4.5 and CLM5: Community Land Model version 4.5 and 5; CTEM: Canadian Terrestrial Ecosystem Model; JSBACH: Jena Scheme for Biosphere-Atmosphere Coupling in Hamburg; SPITFIRE: Spread and InTensity fire model; JULES: Joint UK Land Environment Simulator; INFERNO: Interactive Fire And Emission Algorithm For Natural Environments; GlobFIRM: fire module Global FIRe Model; SMIFIRE: SIMple FIRE model; BLAZE: Blaze-Induced Land-Atmosphere Flux Estimator; ORCHIDEE: Organizing Carbon Hydrology In Dynamic Ecosystems; PFT: plant functional type; P: prescribed; M: modeled

Table 2. Summary description of global fire modules in FireMIP DGVMs

DGVMs	nat. veg. dist.	pastures	crop fire	tropical human defor. fire	human ignition	human fire suppression	peat fire	combust. complete. range of woody tissue
CLM4.5	P	as natural grassland	yes	yes	increase with PD[a]	occurrenc & spread area[b]	yes[e]	27–35% (stem) 40% (CWD[f])
CTEM	P	as natural grassland	no	no	increase with PD	occurrence & duration[c]	no	6% (stem) 15–18% (CWD)
JSBACH	P	high fuel bulk dens.	no	no	increase with PD	occurrence & duration[c]	no	0–45%
JULES	M	as natural grassland	no	no	increase with PD	occurrence[c]	no	0–40%
LGG	M	harvest	no	no	no	no	no	70–90%
LGS	M	as natural grassland	as grass fire	no	increase with PD	occurrence[c]	no	0–98% (100h[g]) 0–80% (1000h[g])
LGSB	M	harvest	no	no	increase with PD	burned area[c]	no	0–50%
MC2	M	as natural grassland	no	no	no	occurrence[d]	no	0–87% (100h) 0–43% (1000h)
ORCHIDEE	P	as natural grassland	no	no	increase with PD	occurrence[c]	no	0–73% (100h) 0–41% (1000h)

[a] PD: population density

[b] fire suppression increases with PD and GDP, different between tree PFTs and grass/shrub PFTs

[c] fire suppression increases with PD

[d] Assume no fire in grid cell when pre-calculated rate of spread, fireline intensity, and energy release component are lower than thresholds

[e] CLM4.5 outputs in FireMIP include biomass and litter burning due to peat fires, but don't include burning of soil organic matter

[f] Coarse Woody Debris

[g] 100-hour fuels and 1000-hour fuel classes

Table 3. Emission factors (g species (kg DM)$^{-1}$) for land cover types (LCTs).

No.	Species	grassland /savanna	tropical forest	temperate forest	boreal forest	cropland
1	CO_2	1647	1613	1566	1549	1421
2	CO	70	108	112	124	78
3	CH_4	2.5	6.3	5.8	5.1	5.9
4	NMHC	5.5	7.1	14.6	5.3	5.8
5	H2	0.97	3.11	2.09	1.66	2.65
6	NO_x	2.58	2.55	2.90	1.69	2.67
7	N_2O	0.18	0.20	0.25	0.25	0.09
8	$PM_{2.5}$	7.5	8.3	18.1	20.2	8.5
9	TPM	8.5	10.9	18.1	15.3	11.3
10	TPC	3.4	6.0	8.4	10.6	5.5
11	OC	3.1	4.5	8.9	10.1	5.0
12	BC	0.51	0.49	0.66	0.50	0.43
13	SO_2	0.51	0.78	0.75	0.75	0.81
14	C_2H_6 (ethane)	0.42	0.94	0.71	0.90	0.76
15	CH_3OH (methanol)	1.48	3.15	2.13	1.53	2.63
16	C_3H_8 (propane)	0.14	0.53	0.29	0.28	0.20
17	C_2H_2 (acetylene)	0.34	0.43	0.35	0.27	0.32
18	C_2H_4 (ethylene)	1.01	1.11	1.22	1.49	1.14
19	C_3H_6 (propylene)	0.49	0.86	0.67	0.66	0.48
20	C_5H_8 (isoprene)	0.12	0.22	0.19	0.07	0.18
21	$C_{10}H_{16}$ (terpenes)	0.10	0.15	1.07	1.53	0.03
22	C_7H_8 (toluene)	0.20	0.23	0.43	0.32	0.18
23	C_6H_6 (benzene)	0.34	0.38	0.46	0.52	0.31
24	C_8H_{10} (xylene)	0.09	0.09	0.17	0.10	0.09
25	CH_2O (formaldehyde)	1.33	2.40	2.22	1.76	1.80
26	C_2H_4O (acetaldehyde)	0.86	2.26	1.20	0.78	1.82
27	C_3H_6O (acetone)	0.47	0.63	0.70	0.61	0.61
28	$C_3H_6O_2$(hydroxyacetone)	0.52	1.13	0.85	1.48	1.74
29	C_6H_5OH (Phenol)	0.37	0.23	0.33	2.96	0.50
30	NH_3 (ammonia)	0.91	1.45	1.00	2.82	1.04
31	HCN (hydrogen cyanide)	0.42	0.38	0.62	0.81	0.43
32	MEK/2-butanone	0.13	0.50	0.23	0.15	0.60
33	CH_3CN (acetonitrile)	0.17	0.51	0.23	0.30	0.25

Table 4. Attribution of plant function types (PFTs) in FireMIP DGVMs to land cover types (LCTs) for emission factors described in Table 2.

LCT / Models	Grassland /Savannas	Tropical Forest	Temperate Forest	Boreal Forest	Cropland
CLM4.5	A C3/C3/C4 G	Tro BE T	Tem NE T	Bor NE T	Crop
	Bor BD S	Tro BD T	Tem BE T	Bor ND T	
	Tem BE/BD S		Tem BD T	Bor BD T	
CTEM	C3/C4 G	BE T[a]	NE/BE T[a]	NET[a], ND T	C3/C4 Crop
		Other BD T[a]	Other BD T[a]	Cold BD T	
JSBACH	C3/C4 G/P	Tro E/D T	Ex-Tro E/D T[a]	Ex-Tro E/D T[a]	Crop
JULES	C3/C4 G	Tro BE T	Tem BE T	BD/NE T[a]	
	E/D S	BD T[a]	BD/NE T[a]	NDT	
LGG[b]	C3/C4 G	Tro BE/BR T	Tem NSG/BSG/BE T	Bor NE T	R/I S/W Wheat
	C3/C4 G in P	Tro SI BE T	Tem SI SG B T	Bor SI NE T	R/I Maize
LGS	C3/C4 G	Tro BE/BR T	Tem SI/&SG B T	Bor NE T	
		Tro SI BE T	Tem B/N E T	Bor SI/&SG NE/N T	
LGSB[b]	C3/C4 G	Tro BE/BR T	Tem NSG/BSG/ BE T	Bor NE T	R/I S/W Wheat
	C3/C4 G in P	Tro SI BE T	Tem SI SG B T	Bor SI NE T	R/I Maize
MC2	Tem C3 G/S	Tro BE T	Maritime NE F	Bor NE F	
	Sub-Tro C4 G/S	Tro D W[c]	Sub-Tro NE/BD/BE/M F	Subalpine F	
	Tro S/G/Sava		Tem NE/BD F	Cool N F	
	Bor M W		Tem C/W M F		
	Tem/Sub-Tro NE/B/M W				
	Tundra				
	Taiga-Tundra				
ORCHIDEE	C3/C4 G	Tro B E/R T	Tem N/B E T	Bor N E/D T	C3/C4 Crop
			Tem BD T	Bor BT T	

Acronym: T: tree; S: shrub; W: woodland; F: forest; G: grass; P: pasture; Sava: Savanna; N: needleleaf; E: evergreen; B: broadleaf; D: deciduous; R: raingreen; SI: shaded-intolerant; SG: summer-green; M: mixed; I: irrigated; RF: rainfed; C/W: cool or warm; S/W: spring or winter, Tro: Tropical; Tem: Temperate; Bor: Boreal; Sub-Tro: subtropical; Ex-Tro: Extratropical; A: Arctic

[a] split tree PFTs into tropical, temperate, and boreal groups following rules of Nemani and Running (1996) that also used to make CLM land surface data by Peter et al. (2007; 2012) since CLM version 3

[b] LGG and LGBS did not outputs PFT-level fire carbon emissions, so land cover classified using its dominant vegetation type

[c] MC2 classifies tropical savannas and tropical deciduous woodland regions, and the latter mainly represents tropical deciduous forests

Table 5. Summary description of satellite-based products and historical constructions merged from multiple sources.

Name	Method	Fire data sources	Peat burning	Start year	reference
GFED4	Bottom-up: fuel consumption,	MODIS,VIRS/ATSR	Y	1997	van der Werf et al. (2017)
GFED4s	burned area &active fire counts		Y	1997	
GFAS1.2	(GFED4&4s), FRP (GFAS1),	MODIS	Y	2001	Kaiser et al. (2012)
FINN1.5	active fire counts (FINN1.5), emis. factor	MODIS	N	2003	Wiedinmyer et al. (2011)
FEER1	Top-down: FRP, satellite AOD	MODIS, SEVIRI	Y	2003	Ichoku and Ellison (2014)
QFED2.5	constrained, emis. factor	MODIS	N	2001	Darmenov and da Silva (2015)
CMIP5	Merged decadal fire trace gas and aerosol emis.	GFED2, GICC, RETRO (model GlobFIRM used)	Y	1850	Lamarque et al. (2010)
CMIP6	Merged monthly fire carbon emis., present-day veg. dist., emis. factor	GFED4s, median of six FireMIP model sims., GCDv3 charcoal records, WMO visibility obs.	Y	1750	van Marle et al. (2017)

Acronym: GFED4: Global Fire Emissions Dataset version 4; GFED4s: GFED4 with small fires; GFAS1.2: Global Fire Assimilation System version 1.2; FINN1.5: Fire Inventory from NCAR version 1.5; FRP: fire radiative power; FEER1: Fire emissions from the Fire Energetics and Emissions Research version1; QFED2.5: Quick Fire Emissions Dataset version 2.5; AOD: aerosol optical depth; GFED2: GFED version 2; RETRO: REanalysis of the TROpospheric chemical composition; GICC: Global Inventory for Chemistry-Climate studies; GCDv3: Global Charcoal Database version 3

Table 6. Global total of fire emissions from 2003 to 2008 for DGVMs in FireMIP and benchmarks. Unit: Pg (Pg=10^{15}g)

Source	C	CO_2	CO	CH_4	BC	OC	$PM_{2.5}$
FireMIP							
CLM4.5	2.1	6.5	0.36	0.018	0.0021	0.020	0.042
CTEM	3.0	8.9	0.48	0.025	0.0028	0.030	0.060
JSBACH	2.1	6.5	0.32	0.013	0.0020	0.016	0.036
JULES	2.1	6.9	0.44	0.024	0.0022	0.020	0.039
LGG	4.9	15.4	0.90	0.047	0.0050	0.048	0.097
LGS	1.7	5.6	0.26	0.011	0.0017	0.012	0.027
LGSB	2.5	7.7	0.48	0.025	0.0025	0.024	0.047
MC2	1.0	3.1	0.18	0.008	0.0011	0.012	0.025
ORCHIDEE	2.8	9.2	0.44	0.018	0.0029	0.020	0.045
Benchmarks							
GFED4	1.5	5.4	0.24	0.011	0.0013	0.012	0.025
GFED4s	2.2	7.3	0.35	0.015	0.0019	0.016	0.036
GFAS1.2	2.1	7.0	0.36	0.019	0.0021	0.019	0.030
FINN1.5	2.0	7.0	0.36	0.017	0.0021	0.022	0.039
FEER1	4.2	14.0	0.65	0.032	0.0042	0.032	0.054
QFED2.5	----	8.2	0.39	0.017	0.0060	0.055	0.086

Table 7. Temporal correlation of annual global fire $PM_{2.5}$ emissions between FireMIP models and satellite-based GFED4 and GFED4s (1997–2012), GFAS1.2 and QFED2.5 (2001–2012), and FINN1.5 and FEER1 (2003–2012).

DGVMs	GFED4	GFED4s	GFAS1.2	FINN1.5	FEER1	QFED2.5
CLM4.5	0.73***	0.79***	0.63**	0.62*	0.55*	0.58**
CTEM	0.51**	0.54**	0.63**	0.60*	0.52	0.68**
JSBACH	–0.18	–0.42	0.10	0.02	–0.04	0.32
JULES	0.33	0.31	0.31	0.56*	0.29	0.39
LGG	0.08	0.03	–0.15	0.01	–0.20	–0.03
LGS	0.12	0.04	–0.00	0.40	–0.01	0.08
LGSB	0.51**	0.64***	0.39	0.72**	0.56*	0.55*
ORCHIDEE	–0.13	–0.25	–0.16	0.29	–0.10	–0.10

*,**,and *** : Pearson correlation passed the Student's t-test at the 0.1, 0.05, and 0.01 significance level, respectively.

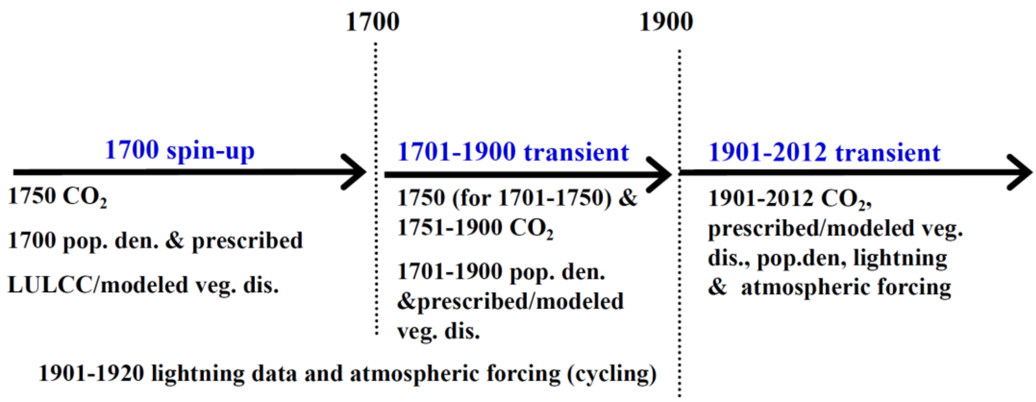

Figure 1. FireMIP experiment design. Note that CTEM and MC2 start at 1861 and 1901 and spin-up using 1861 and 1901 CO2, population density, and prescribed / modeled vegetation distribution, respectively.

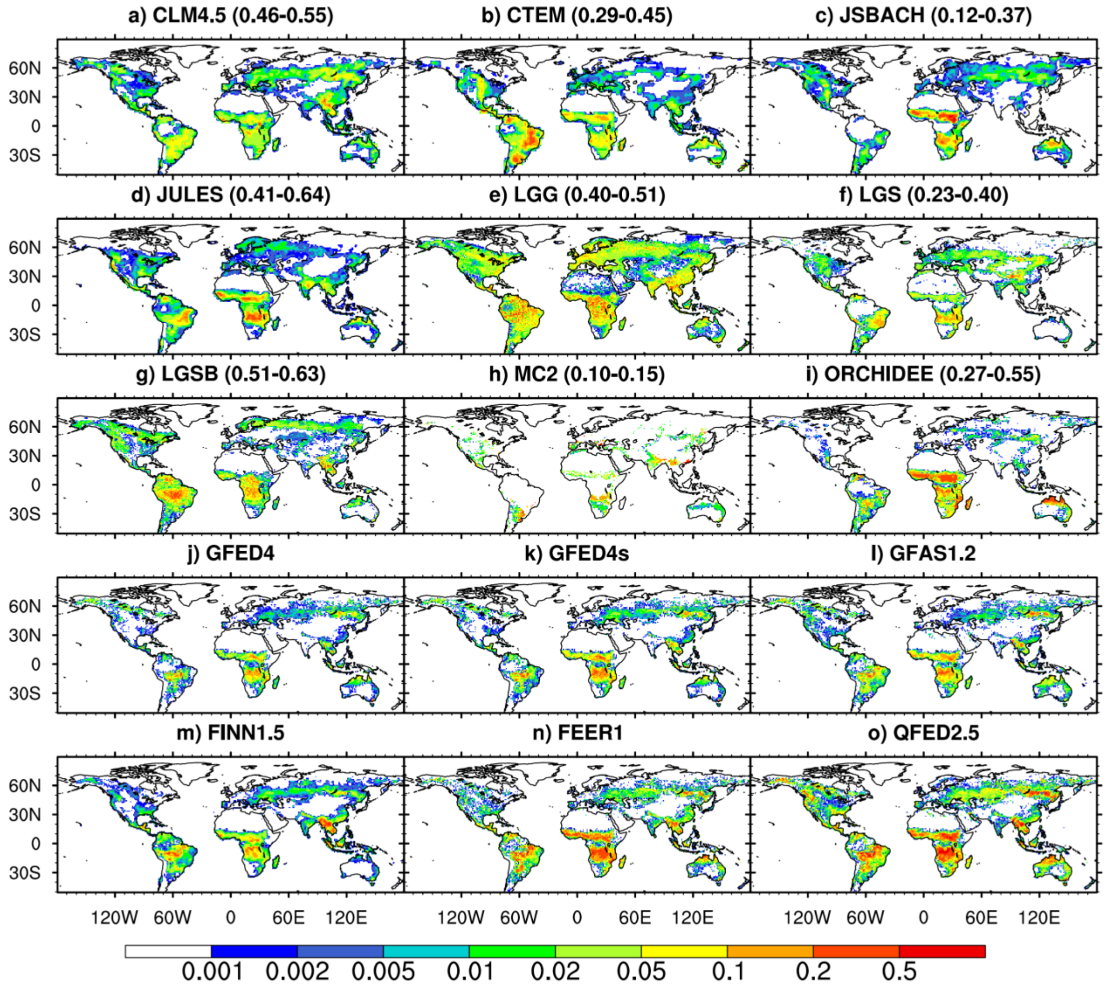

Figure 2. Spatial distribution of annual fire black carbon (BC) emissions (g BC m^{-2} yr^{-1}) averaged over 2003–2008. The range of global spatial correlation between DGVMs and satellite-based products is also given in brackets.

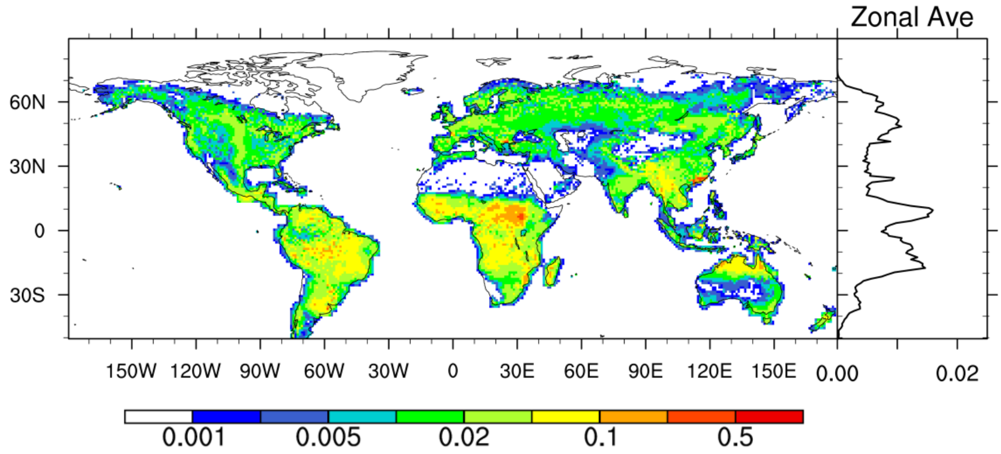

Figure 3. Inter-model standard deviation of 2003–2008 averaged fire BC emissions (g BC m^{-2} yr^{-1}) in FireMIP models and the zonal average.

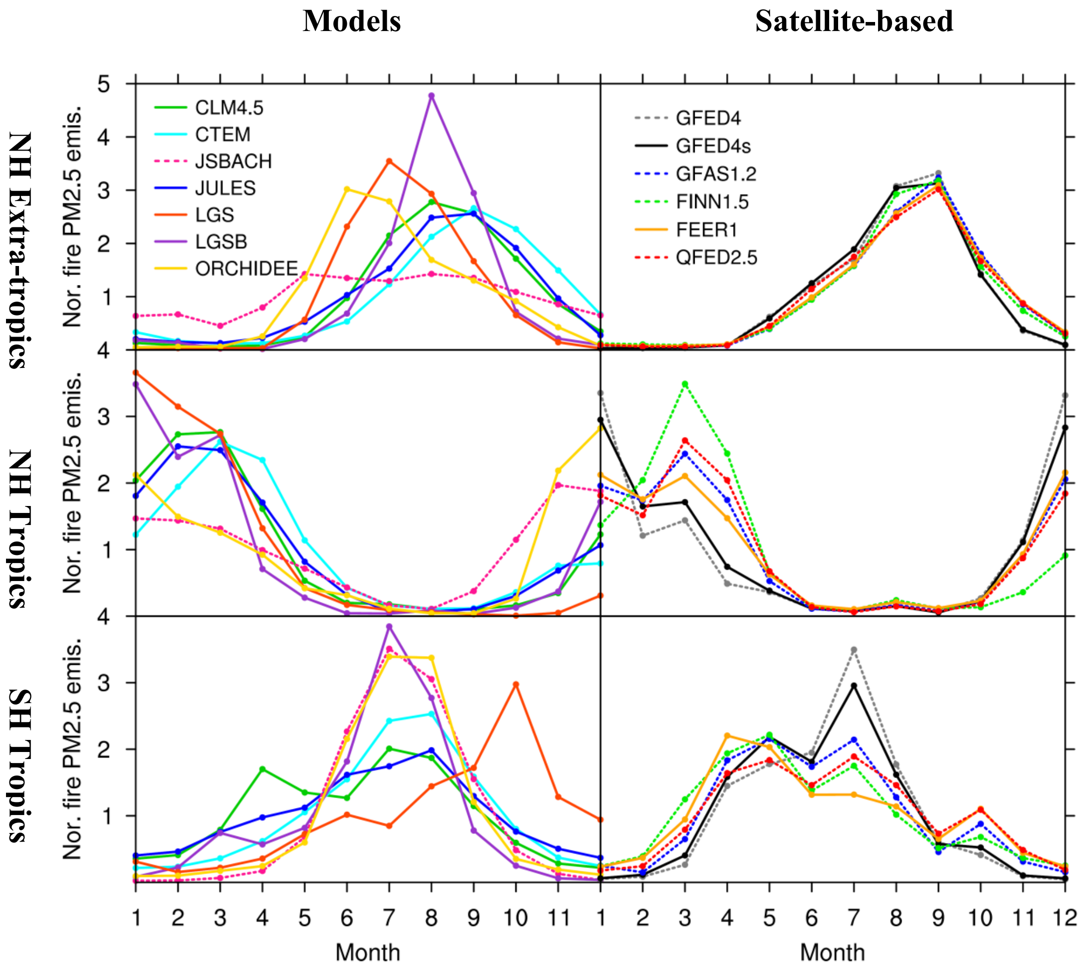

Figure 4. Seasonal cycle of fire $PM_{2.5}$ emissions normalized by the mean from FireMIP models and satellite-based products averaged over 2003–2008 in the Southern Hemisphere (SH) tropics (0–23.5ºS), Northern Hemisphere (NH) tropics (0–23.5ºN), and NH extra-tropics (23.5–90ºN). Fire emissions from LPJ-GUESS-GlobFIRM and MC2 are updated annually and thus are not included here.

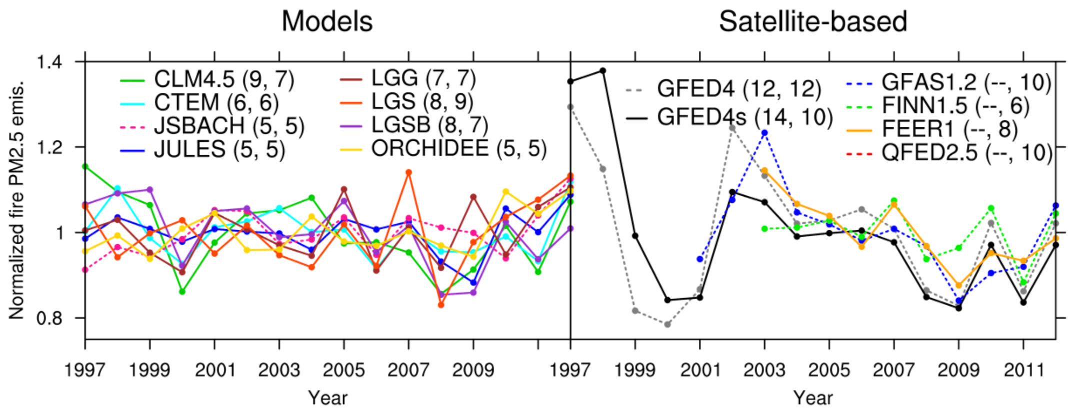

Figure 5. Temporal change of annual global fire $PM_{2.5}$ emissions normalized by the mean from FireMIP models and satellite-based products. The numbers in the brackets are coefficient of variation (CV, the standard deviation divided by the mean, unit: %) for 1997–2012 and 2003–2012, respectively.

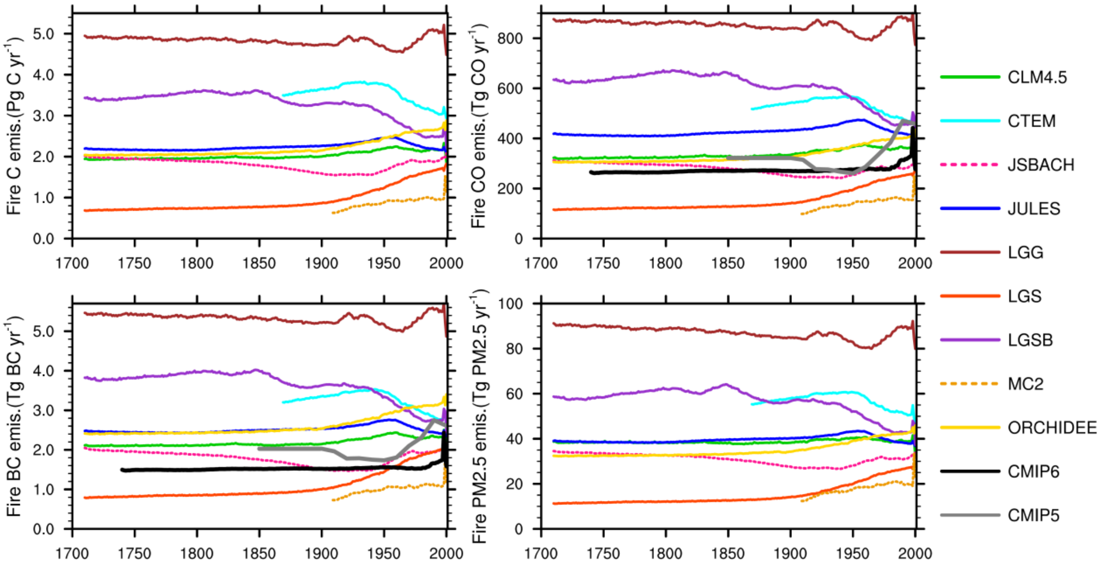

Figure 6. Long-term temporal change of fire emissions from DGVMs in FireMIP and CMIPs forcing. A 21-year running mean is used.

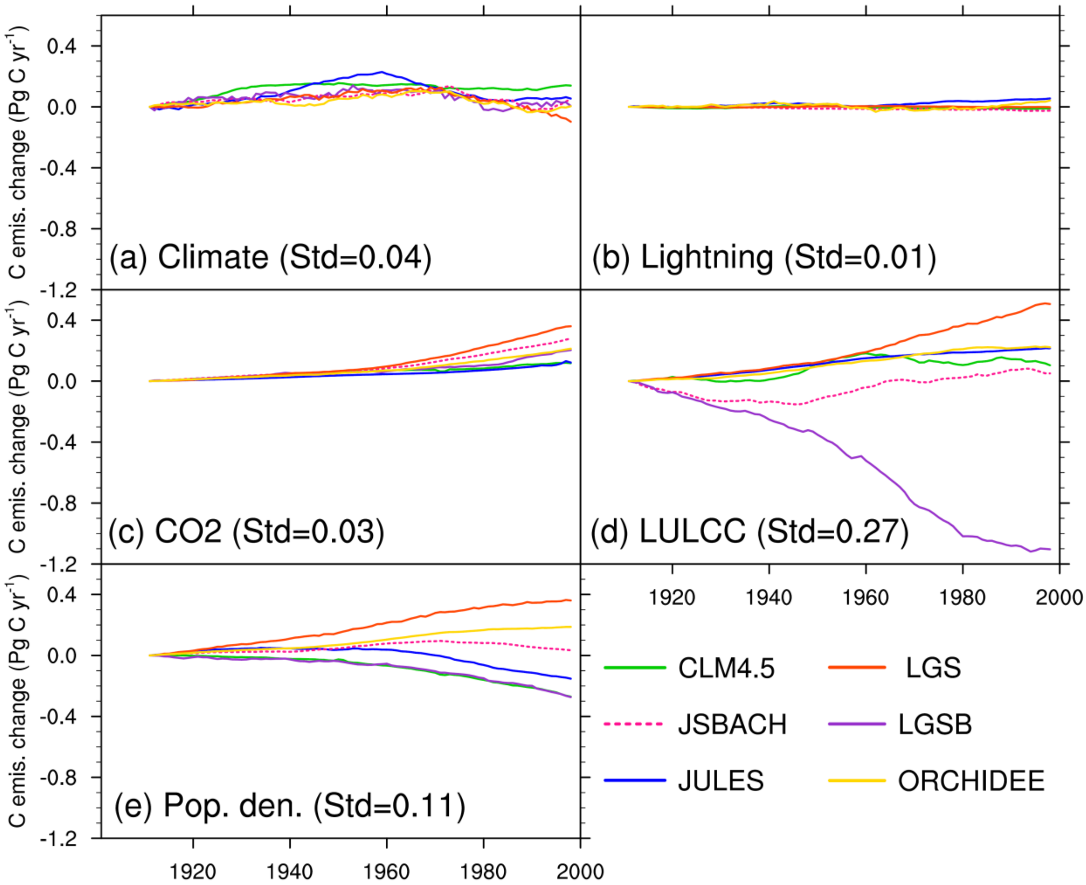

Figure 7. Change in global annual fire carbon emissions (Pg C yr^{-1}) in the 20^{th} century due to changes in (a) climate, (b) lightning frequency, (c) atmospheric CO_2 concentration, (d) land use and land cover change (LULCC), and (e) population density (control run – sensitivity run). A 21-year running mean is used. The standard deviation (Std) of multi-model simulated long-term changes averaged over the 20^{th} century is also given in the bracket.

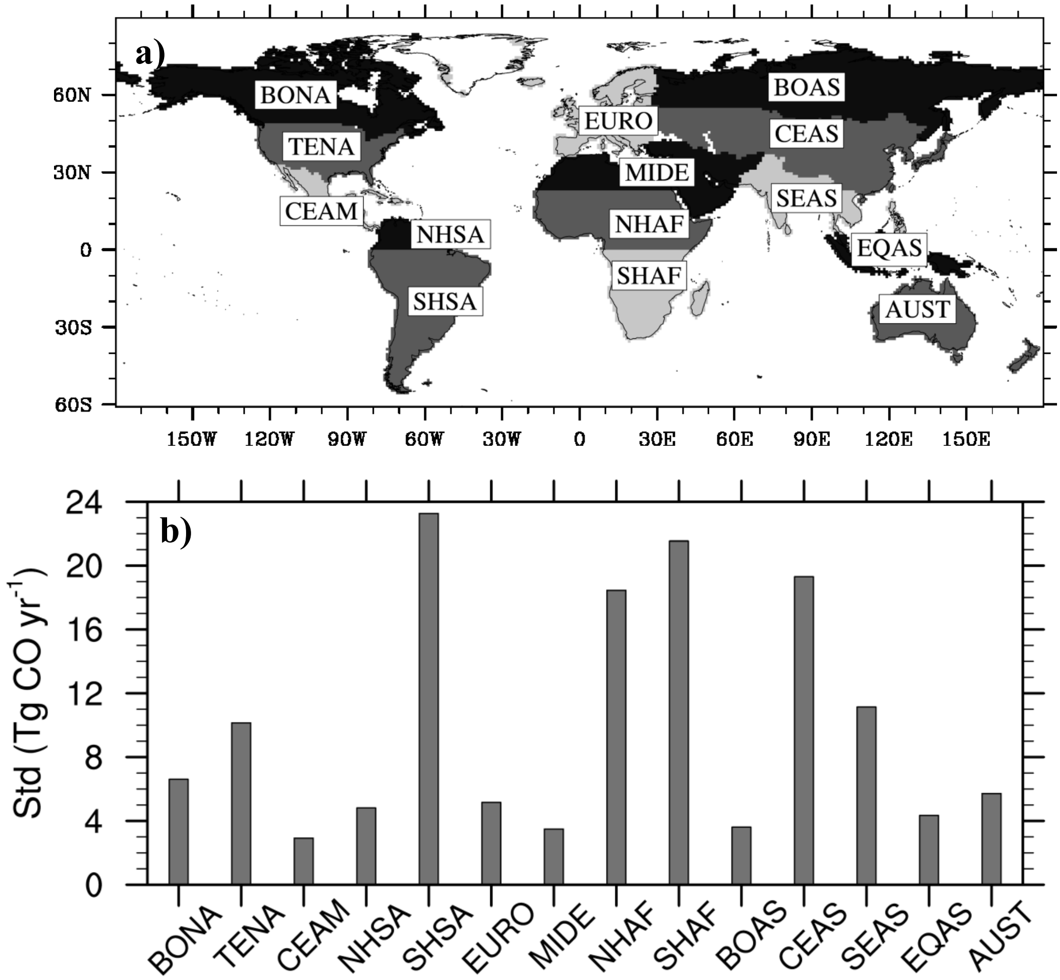

Figure 8. a) GFED region definition (http://www.globalfiredata.org/data.html), and b) inter-model discrepancy (quantified using inter-model standard deviation) in long-term changes (a 21-year running mean is used, relative to present-day) of simulated regional fire CO emissions (Tg CO yr^{-1}) averaged over 1700–2012 (calculate long-term changes relative to present-day for each FireMIP model first, then the inter-model standard deviation, and lastly the time-average). Acronyms are BONA: Boreal North America; TENA: Temperate North America; CEAM: Central America; NHSA: Northern Hem. South America; SHSA: Southern Hem. South America; EURO: Europe; MIDE: Middle East; NHAF: Northern Hem. Africa; SHAF: Southern Hem. Africa; BOAS: Boreal Asia; CEAS: Central Asia; SEAS: Southeast

Asia; EQAS: Equatorial Asia; AUST: Australia.

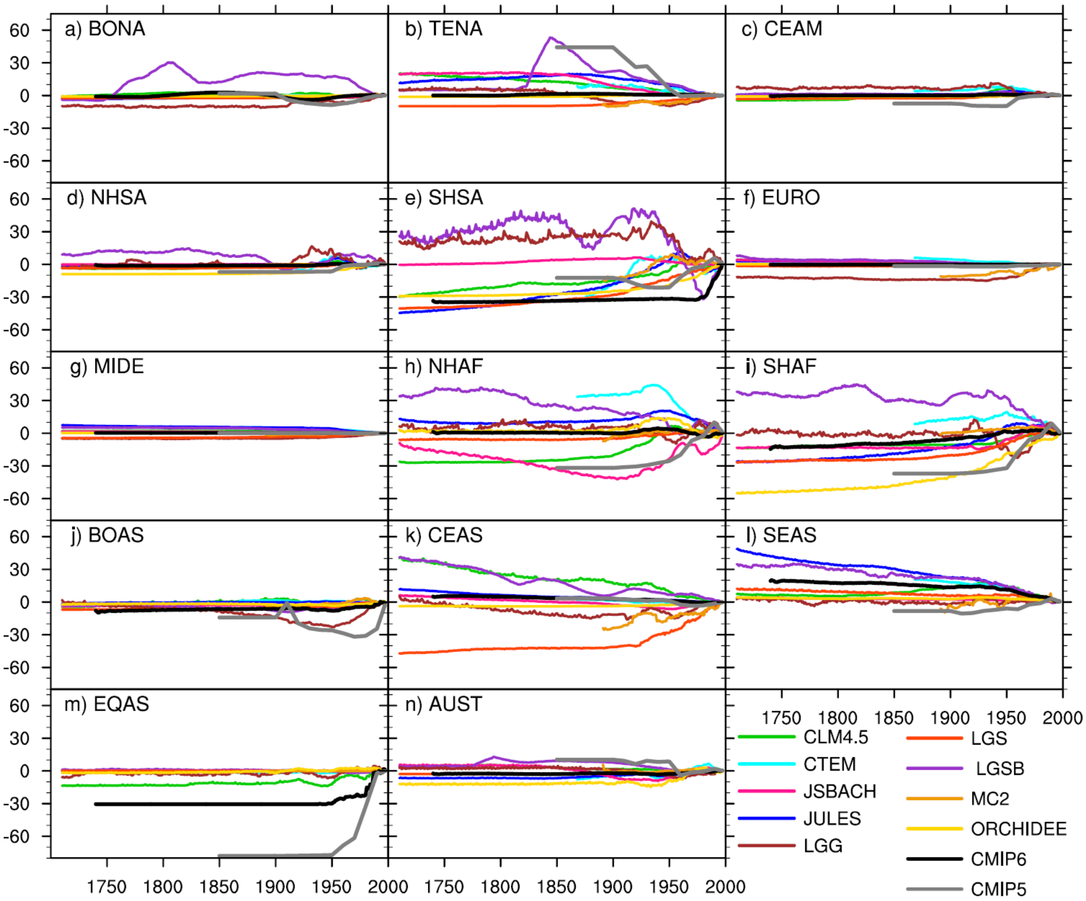

Figure 9. Long-term changes of annual regional fire CO emissions (Tg CO yr^{-1}) from FireMIP models and CMIPs. A 21-year running mean is used.